TransCom N_2O model inter-comparison Part I: Assessing the influence of transport and surface fluxes on tropospheric N_2O variability

R. L. Thompson[1,2], P. K. Patra[3], K. Ishijima[3], E. Saikawa[4,5], M. Corazza[6], U. Karstens[7], C. Wilson[8], P. Bergamaschi[6], E. Dlugokencky[9], C. Sweeney[9], R. G. Prinn[4], R. F. Weiss[10], S. O'Doherty[11], P. J. Fraser[12], L. P. Steele[12], P. B. Krummel[12], M. Saunois[2], M. Chipperfield[8] and P. Bousquet[2]

1. Norwegian Institute for Air Research, Kjeller, Norway
2. Laboratoire des Sciences du Climat et l'Environnement, Gif sur Yvette, France
3. Research Institute for Global Change, JAMSTEC, Yokohama, Japan
4. Center for Global Change Science, MIT, Cambridge, MA, USA
5. Department of Environmental Studies, Emory University, GA, USA
6. Institute for Environment and Sustainability, Joint Research Centre, European Commission, Ispra, Italy
7. Max Planck Institute for Biogeochemistry, Jena, Germany
8. School of Earth and Environment, University of Leeds, Leeds, United Kingdom
9. NOAA Earth System Research Laboratory, Global Monitoring Division, Boulder, CO, USA
10. Scripps Institution of Oceanography, La Jolla, CA, USA
11. Atmospheric Chemistry Research Group, School of Chemistry, University of Bristol, Bristol, United Kingdom
12. Centre for Australian Weather and Climate Research, CSIRO, Marine and Atmospheric Research, Aspendale, Victoria, Australia

Abstract

We present a comparison of chemistry-transport models (TransCom-N_2O) to examine the importance of atmospheric transport and surface fluxes on the variability of N_2O mixing ratios in the troposphere. Six different models and two model variants participated in the inter-comparison and simulations were made for the period 2006 to 2009. In addition to N_2O, simulations of CFC-12 and SF_6 were made by a subset of four of the models to provide information on the models proficiency in stratosphere-troposphere exchange (STE) and meridional transport, respectively. The same prior emissions were used by all models to restrict differences among models to transport and chemistry alone. Four different N_2O flux scenarios totalling between 14 and 17 TgN y^{-1} (for 2005) globally were also compared. The modelled N_2O mixing ratios were assessed against observations from in-situ stations, discrete air sampling networks, and aircraft. All models adequately captured the large-scale patterns of N_2O and the vertical gradient from the troposphere to the stratosphere and most models also adequately captured the N_2O tropospheric growth rate. However, all models underestimated the inter-hemispheric N_2O gradient by at least 0.33 parts-per-billion (ppb), equivalent to 1.5

TgN, which, even after accounting for an overestimate of emissions in the Southern Ocean of circa 1.0 TgN, points to a likely underestimate of the Northern Hemisphere source by up to 0.5 TgN and/or an overestimate of STE in the Northern Hemisphere. Comparison with aircraft data reveal that the models overestimate the amplitude of the N_2O seasonal cycle at Hawaii (21°N, 158°W) below circa 6000 m, suggesting an overestimate of the importance of stratosphere to troposphere transport in the lower troposphere at this latitude. In the Northern Hemisphere, most of the models that provided CFC-12 simulations captured the phase of the CFC-12, seasonal cycle, indicating a reasonable representation of the timing of STE. However, for N_2O all models simulated a too early minimum by 2 to 3 months owing to errors in the seasonal cycle in the prior soil emissions, which was not adequately represented by the terrestrial biosphere model. In the Southern Hemisphere, most models failed to capture the N_2O and CFC-12 seasonality at Cape Grim, Tasmania, and all failed at the South Pole, whereas for SF_6, all models could capture the seasonality at all sites, suggesting that there are large errors in modelled vertical transport in high southern latitudes.

1. Introduction

Nitrous oxide (N_2O) mixing ratios have been increasing steadily in the atmosphere over the past few decades at an average rate of approximately 0.3% per year, reaching 323 nmol mol^{-1} (equivalently parts-per-billion, ppb) in recent years (WMO, 2011) compared with circa 270 ppb before the industrial revolution (Forster et al., 2007). The growth rate of N_2O is a direct consequence of the imbalance between the emission and the sink of N_2O. The sink, that is, photolysis and oxidation by $O(^1D)$ in the stratosphere, is thought to have increased at a slower rate than that of the emissions, which have been increasing since the mid-19^{th} century largely due to human activities. N_2O emissions are strongly tied to the amount of reactive nitrogen (ammonium, nitrate and organic forms) in the environment. The global demand for food, and more recently bio-fuels, has led to an increasing production of reactive nitrogen, used in fertilizers, especially in the latter half of the 20^{th} century (Galloway et al., 2008). The increase in N_2O is a major concern because it is a greenhouse gas (GHG) and has the third largest contribution to anthropogenic radiative forcing after CO_2 and CH_4 (Butler, 2011). Additionally, N_2O plays an important role in stratospheric ozone loss and the ozone-depleting-potential weighted emissions of N_2O are now thought to be the largest of all ozone depleting substances (Ravishankara et al., 2009).

Despite the importance of N_2O, there are still many questions concerning the causes of its seasonal and, especially, inter-annual variability in the atmosphere and there are still large uncertainties in its emission. Understanding of the seasonal variability of N_2O has improved in recent years with the recognition of the importance of seasonal stratosphere-troposphere exchange (STE) of air masses on the tropospheric seasonal cycle observed at a number of sites (Nevison et al., 2007; Nevison et al., 2011). However, there is still some debate about the additional contribution of surface fluxes and lateral transport to the seasonal cycle and the latitudinal dependence of this (Ishijima et al., 2010). Similarly, inter-annual variability in STE has been suggested to be an important determinant of inter-annual variability in tropospheric N_2O (Nevison et al., 2011), however, recent studies point to a greater importance of tropospheric transport and variations in surface emissions (Saikawa et al., 2013; Thompson et al., 2013; Thompson et al. 2014a).

N_2O emissions can be estimated from atmospheric observations with the use of an atmospheric chemistry transport model (CTM) to translate between concentrations and fluxes. This is formalized in atmospheric inversions, where the estimated fluxes are those that provide the best fit to the observations while remaining within the bounds of the prior flux estimate and the assigned uncertainties. However, extracting information about N_2O fluxes from atmospheric observations is extremely challenging owing to the small signal to noise ratio of these measurements. For instance, the typical precision on a discrete air sample is about 0.3 ppb while the annual mean inter-hemispheric gradient is 1.4 ppb. In addition, there are complications of atmospheric transport, in particular, STE (Nevison et al., 2011). This is one of the main motivations for this study, i.e., to investigate what can be learnt from atmospheric measurements of N_2O and to what extent these can advance knowledge about surface fluxes. Simulations of N_2O using CTMs can help our understanding of the influence of transport on N_2O spatial and temporal variability. Ultimately though, our knowledge about N_2O emissions through atmospheric inversions will only improve with a quantification of the uncertainties in modelled atmospheric transport and in the prior emissions.

TransCom is a community that was established in the early 1990s primarily to examine the performance of CTMs. Early studies included verification of transport using the anthropogenic tracer SF_6 (Denning et al., 1999) and examining simulations of atmospheric CO_2 (Law et al., 1996; Law et al., 2008). More recently, there was a TransCom study to investigate the roles of emissions, transport and chemical loss on CH_4 (Patra et al., 2011). In

this TransCom study, we examine the influence of emissions, tropospheric transport and STE on the variability in atmospheric N_2O. In particular, we focus on annual to seasonal time-scales. Additionally, we aim to assess the influence of atmospheric transport errors on modelled N_2O concentrations, which are used in the interpretation of inverse modelling results for N_2O emissions (discussed in a companion paper: Thompson et al. 2014b). Six different models and two model variants are included in this forward inter-comparison study and five atmospheric inversion models are included in the inversion study.

In section 2, we describe the atmospheric observations used in the inter-comparison and give details about the models that participated in this study as well as about the study's protocol. Following this, in section 3.1, we present the inter-comparison of large-scale transport features such as the inter-hemispheric (IH) gradient and cross-tropopause gradient. In section 3.2, we examine the tropospheric N_2O seasonal cycle and use comparisons with SF_6 and CFC-12 to help disentangle the contributions from STE, tropospheric transport and surface emissions on N_2O concentrations. CFC-12 has been previously used as a tracer for STE (Nevison et al., 2007) as it has comparatively well known emissions, which have little seasonal variability but, like N_2O, it is only lost in the stratosphere. SF_6 is a useful tracer for tropospheric transport, as it also has comparatively well known emissions, which are largely in the Northern Hemisphere (NH) and it can be treated as inert since it has an estimated lifetime of between 800 and 3200 years (Morris et al., 1995; Ravishankara et al., 1993). Lastly, in section 4, we discuss what can be learnt about N_2O emissions from model-observation comparisons and the implications of atmospheric transport uncertainties for N_2O emission estimates from inversions.

2. Observations, models and methods

2.1 Modelling protocol

A schematic overview of the modelling protocol is shown in Fig. 1 with the different components of the model set-up. To facilitate the analysis of the results in terms of atmospheric transport, all modelling groups were requested to use the same prior fluxes (for N_2O, SF_6 and CFC-12) and the same magnitude for the stratospheric sinks of N_2O and CFC-12. On the other hand, each transport model was used with its own meteorological analysis data or, alternatively, meteorological fields nudged to analysis data in offline atmospheric transport runs (see Table 1). Since each transport model has different vertical and horizontal resolution, each model was also used with its own initial 3D mixing ratio fields.

For simulations of N_2O, it was necessary to account for the loss of N_2O in the stratosphere due to photolysis (circa 90% of the loss) and oxidation by $O(^1D)$ (circa 10% of the loss) (Minschwaner et al., 1993). These processes can be summarized by the following 3 equations:

$$N_2O \xrightarrow{h\nu} N_2 + O^1D \quad \text{(R1)}$$

$$N_2O + O^1D \xrightarrow{k_1} 2NO \qquad (k_1 = 6.7\times10^{-11}\ cm^3\ molecule^{-1}\ s^{-1}) \quad \text{(R2)}$$

$$N_2O + O^1D \xrightarrow{k_2} N_2 + O_2 \qquad (k_2 = 4.4\times10^{-11}\ cm^3\ molecule^{-1}\ s^{-1}) \quad \text{(R3)}$$

Losses of N_2O were calculated on the basis of these equations within each CTM for every grid-cell and time-step. Although the exact photolysis and oxidation rates varied between models, these were scaled such that the global annual total loss of N_2O was approximately 12.5 TgN, consistent with estimates of the atmospheric abundance and the lifetime of N_2O, which is estimated to be between 124 and 130 years (Prather et al., 2012; Volk et al., 1997). Similarly, for models participating in the CFC-12 inter-comparison, it was necessary to account for photolysis of CFC-12 in the stratosphere (R4), which accounts for 93 to 97% of the total loss (Seinfeld and Pandis, 1998). This was done in the same way as for N_2O, that is, the photolysis rates were scaled to be consistent with a CFC-12 lifetime of circa 100 years.

$$CF_2Cl_2 \xrightarrow{h\nu} CFCl + Cl\cdot \quad \text{(R4)}$$

Model simulations were made using meteorology and surface emissions for the period from 1 January 2005 to 31 December 2009, with 2005 being considered as a "spin-up" year and was, therefore, not included in the analysis. A 1-year spin-up was considered sufficient as all models started already with their best-estimated initial conditions taken from previous model integrations.

2.2 Prior fluxes

Four different N_2O emission scenarios were provided to investigate the influence of varying terrestrial and ocean fluxes. All scenarios were comprised of fluxes from the terrestrial biosphere, oceans, biomass burning, waste, fuel combustion and industry and differed only in the estimate of either the terrestrial biosphere or the ocean fluxes (see Tables 2 and 3). Each component flux used to build the scenarios is described below (these were originally provided at monthly temporal and 1.0° × 1.0° spatial resolution unless otherwise stated):

1. Terrestrial biosphere: includes fluxes from natural and cultivated ecosystems from the Orchidee O-CN terrestrial biosphere model (Zaehle and Friend, 2010). The model is

driven by climate data (CRU-NCEP) and inter-annually varying N inputs. Data were originally provided at 3.75° × 2.5° (longitude by latitude) resolution. These fluxes are referred to as OCN.

2. Natural ecosystem: fluxes from uncultivated ecosystems from the empirical model of Bouwman et al. (2002). These fluxes are annual only and are a climatological mean.
3. Agriculture: fluxes from cultivated ecosystems from EDGAR-4.1 at annual resolution (Emission Database for Greenhouse gas and Atmospheric Research, available at: http://edgar.jrc.ec.europa.eu/index.php). These fluxes together with the natural ecosystem fluxes of Bouwman et al. (2002) are referred to as BWM.
4. Waste, combustion and industry: fluxes from fossil fuel combustion, industrial solvents, solid and water waste provided by EDGAR-4.1 at annual resolution. (data available at: http://edgar.jrc.ec.europa.eu/index.php)
5. Ocean: three different flux estimates were used. The first estimate, PIC, was taken from the ocean-biogeochemistry model, PISCES (Aumont and Bopp, 2006) with an original non-regular resolution of approximately 2° longitude × 1° latitude. The second and third estimates were based on extrapolations of observations of N_2O partial pressure anomalies in the surface ocean that have been coupled to air-sea gas exchange coefficients. The N95 fluxes use the Nevison et al. (1995) estimate at 1.0° × 1.0° resolution, while the N04 fluxes use the Nevison et al. (2004) estimate at 0.5° × 0.5° resolution.
6. Biomass burning: fluxes from GFED-2.1 (Global Fire Emissions Database; (van der Werf et al., 2010)).

The four flux estimates were then formed using one of the terrestrial biosphere fluxes, OCN or BWM, and one of the ocean fluxes, PIC, N95 or N04, plus the fluxes from biomass burning, waste, combustion and industry. The scenario, OCNPIC, was used as the control scenario and was used for all model-observation comparisons unless otherwise stated.

Emissions of CFC-12 were provided based on the EDGAR-2 estimate but were scaled to the annual global totals estimated by McCulloch et al. (2003). The global emission in e.g. 2006 was 40 Gg y^{-1}. SF_6 emissions were based on the EDGAR-4.1 estimate and were scaled to the top-down global annual totals of Levin et al (2010). The global emission in 2006 was 6.3 Gg y^{-1}. Both CFC-12 and SF_6 emissions were at 1.0° × 1.0° spatial resolution and were linearly interpolated to monthly temporal resolution

2.3 Transport models

Six models and two of their variants participated in the inter-comparison of modelled N_2O mixing ratios and all of these models have also been included in at least one previous TransCom experiment (Law et al. 2008; Patra et al. 2011). The salient features of each transport model, i.e., the horizontal and vertical resolution and meteorological input are given in Table 1. All models used meteorological fields from weather forecast models (MERRA, NCEP, JRA25, and ECMWF) either by interpolating (offline models) or by nudging towards fields of horizontal winds and temperature (online models). Model output was generated at each site used in the analysis (see section 2.4): as an hourly average (ACTMt42l32, ACTMt42l67), a 1.5-hourly average (TM5), an interpolation to the observation time-step (TM3-NCEP, TM3-ERA), or at the closest model time-step to the observation time (in both LMDZ4 and in TOMCAT this is 30 min). Additionally, 3D fields of monthly mean N_2O mixing ratios were archived (higher temporal resolutions were not considered since this study only looks at seasonal and longer timescales and owing to the large file sizes).

2.4 Observations and data processing

Atmospheric observations of N_2O dry-air mole fractions were pooled from three global networks: NOAA CCGG (National Oceanic and Atmospheric Administration, Carbon Cycle and Greenhouse Gases), NOAA HATS (Halocarbons and other Atmospheric Trace Species), and AGAGE (Advanced Global Atmospheric Gases Experiment), as well as from regular aircraft transects made by NOAA (see Table 4 and Fig. S2). Discrete air samples (flasks) taken in the NOAA CCGG network and in aircraft profiles were analysed for N_2O using GC-ECD (Gas Chromatography with an Electron Capture Detector) and are reported on the NOAA-2006A calibration scale (Hall et al., 2007) and have a reproducibility of 0.4 ppb based on the mean difference of flask pairs. Both NOAA HATS and AGAGE operate networks of in-situ GC-ECD instruments. NOAA HATS data are reported on the NOAA-2006A scale (Hall et al., 2007) and have a reproducibility of approximately 0.3 ppb (Thompson et al., 2004) and data from AGAGE are reported on the SIO-1998 scale and have a precision of approximately 0.1 ppb (Prinn et al., 2000). In addition, observations of CFC-12 and SF_6 mole fractions (pmol mol^{-1}, equivalently parts-per-trillion, ppt) were used from the NOAA HATS and AGAGE networks. Both NOAA HATS measurements were made using in-situ GC-ECD while AGAGE measurements of CFC-12 were made using GC-ECD and SF_6 measurements were made with GC Mass Spectrometry (GC-MS). CFC-12 data are reported on the NOAA-

2008 (NOAA HATS) and SIO-2005 (AGAGE) scales and SF_6 data are reported on the NOAA-2006 (NOAA HATS) and SIO-2005 (AGAGE) scales.

Surface measurements were filtered for outliers using an iterative filter removing values that were outside two standard deviations of the mean over a time interval of three months for flask measurements and three days for in-situ measurements. Data were available at approximately hourly resolution for in-situ data and approximately two-weekly resolution for flask data. For N_2O, calibration offsets between networks, and even between in-situ GCs within a network, are considerable compared to the measurement precision; therefore, prior values of these offsets were estimated by comparing timeseries from different networks and added to the observations for the model-observation comparison (see Table 5).

Mean seasonal cycles were calculated for N_2O, CFC-12 and SF_6 by first removing the multi-annual trend, fitted as a second-order polynomial for N_2O and SF_6 and as a third-order polynomial for CFC-12, and then filtering the timeseries for high-frequency noise using a Butterworth filter. The residuals for each month were then averaged over all years. This method was chosen preferentially over methods involving fitting harmonic curves as these parameterizations impose a strong prior form on the seasonal cycle, which may be unrealistic at sites where the cycle has small amplitude and/or is irregular.

3. Results and Discussion

3.1. Large-scale circulation and the influence on N_2O

The atmospheric distribution of N_2O is characterized by a strong cross-tropopause gradient, owing to the loss of N_2O predominantly in the upper stratosphere and STE, and a south to north gradient in the troposphere due to stronger emissions in the NH versus the SH. This section examines these large-scale features in the models and assesses them against observational data. In the following discussion, we refer to stratosphere to troposphere transport (STT) as the transport from the stratosphere to the troposphere, which is not to be confused with stratosphere-troposphere exchange (STE), which is a general term for exchange in both directions.

3.1.1. Zonal mean vertical profile

Figure 2 shows the variation of the annual zonal mean N_2O concentration with pressure and latitude for each model using the control flux estimate, OCNPIC (the general features of the

zonal mean profiles do not differ with the other flux estimates and are, therefore, not shown). Generally, the large-scale features of the N_2O atmospheric gradient are similar in all simulations. However, they vary in the strength of the tropospheric south to north gradient and the gradient across the tropopause and in the stratosphere. The strength of the cross-tropopause gradient is largely determined by the rate of STE, which depends on the strength of the Brewer Dobson circulation as well as on tropopause folding events, cut-off lows, and small-scale mixing associated with upper level fronts and cyclones (Holton et al., 1995). The Brewer-Dobson circulation oscillates seasonally with air ascending diabatically across the tropopause in the tropics, stratospheric poleward transport in the winter hemisphere, and diabatically descending air across the tropopause in the high latitudes in winter (Holton et al., 1995). The seasonal influence of the Brewer Dobson circulation on N_2O mixing ratios is better resolved in MOZART4, ACTMt42l67, TM5, TM3-ERA and TOMCAT than in the models with low vertical resolution (LMDZ4 with only 19-eta layers) and those with few stratospheric layers (ACTMt42l32 and TM3-NCEP) (see Fig. S1).

The stratosphere can be classified into an "overworld" and an "underworld" to better describe STE. The overworld lies entirely above the 380 K isentrope, while the underworld has the tropopause as its lower bound and the 380 K isentrope as its upper bound. Isentropic surfaces intersect the tropopause in the extra-tropics, lying partly in the lower extra-tropical stratosphere and partly in the troposphere. Air masses can thus be mixed adiabatically between the troposphere and lower stratosphere along isentropes that intersect the tropopause (Holton et al., 1995). Since on annual timescales there is no net change in the mass of the lower stratosphere, exchange across the 380 K isentropic surface can be considered as representative of the net STE (Schoeberl, 2004). This is a particularly useful simplification when considering the budgets of species such as N_2O and CFC-12, which have a source in the troposphere and sink in the stratosphere. Table 6 shows the height of the tropopause and the gradients across the tropopause and the 380 K isentropic surface in each model. Tropopause heights were calculated as the height at which the temperature lapse rate becomes less than 2 K km^{-1}, with the added condition that the lapse rate from that height up to 2 km higher must also not exceed 2 K km^{-1}, following the method of Reichler et al. (2003). The height of the tropopause and 380K isentrope is fairly consistent between all models, i.e. within ±4% and ±12% of the mean, respectively. LMDZ4 has the strongest gradients across 380 K isentrope in the tropics and extra-tropics owing to the low vertical resolution, while TM3-NCEP has the weakest gradients owing to strong vertical mixing.

3.1.2. Growth rate and lifetime

The tropospheric growth rate of N_2O is determined by the sum of the surface emissions and the net flux of N_2O across the tropopause and, on annual timescales, across the 380 K isentrope. Since all models use the same prior fluxes (OCNPIC), differences in the modelled growth rates are due directly to differences in the net cross-tropopause N_2O flux, which depend on the upward and downward mass fluxes and on the above and below tropopause N_2O mixing ratios; factors that are determined by the meteorological data used as well as on the vertical definition of the models. Table 7 shows the annual mean (2006 – 2009) tropospheric N_2O growth rates, total abundance, total sink, and the atmospheric lifetime of N_2O. Tropospheric growth rates were calculated in both the models and the observations as the mean growth rate at background surface sites (these were: ZEP, BRW, ALT, SHM, MHD, THD, IZO, KUM, MLO, RPB, CHR, SEY, SMO, ASC, EIC, CGO, TDF, HBA, and SPO, for a description of the sites see Table 4). The total sink was calculated directly by adding up the loss at each timestep (except in ACTMt42l32 where it was calculated as the difference between the total source and the change in total burden) and the lifetime was calculated as the atmospheric N_2O abundance up to approximately 50 hPa divided by the global annual loss. Most models have tropospheric growth rates close to the observed rate of 0.84 ppb y^{-1} with the exceptions of ACTMt42l32 and LMDZ4, which have substantially lower rates. Figure 3 shows the relationship between growth rate and lifetime for the observations and models. Although in ACTMt42l32 the low growth rate can be explained by the anomalously large sink (16 TgN y^{-1}) and correspondingly short lifetime (92 y), in LMDZ4 it is not so straightforward. LMDZ4 has been shown to be a relatively diffuse model with fast venting of the Planetary Boundary Layer (PBL) (Geels et al., 2007), which results in N_2O being mixed too rapidly into higher altitudes and insufficient accumulation of N_2O in the PBL. TOMCAT, despite capturing the growth rate, has a shorter lifetime owing to the low abundance of N_2O in the troposphere and stratosphere. The problems in LMDZ4 and TOMCAT could be rectified at least to some extent by using longer spin-up times, which would bring the vertical gradients closer to steady-state.

3.2. Tropospheric transport

3.2.1. Vertical gradients

Vertical mixing ratio gradients represent the combined influence of surface fluxes and atmospheric transport. For N_2O, the surface fluxes are largely from the land and these are

predominantly positive, therefore, the mixing ratio generally decreases with altitude. Sites located in the interior or downwind of continents show stronger gradients than those downwind of ocean basins owing to the stronger influence of land fluxes. However, at sites where there are only weak surface fluxes, the gradient may be heavily influenced by lateral transport and in some cases become positive in the troposphere. Figure 4 shows the seasonal and annual mean modelled (using the OCNPIC flux scenario) and observed vertical gradients of N_2O mixing ratio at the NOAA GMD aircraft profiling sites: Raratonga (RTA, 21°S, 160°E), Hawaii (HAA, 21°N, 158°W), Ulaanbaatar (ULB, 47°N, 106°E) and Poker Flats (PFA, 65°N, 147°W). For all vertical gradients (from the surface to 6000 m), the mean modelled/observed tropospheric mixing ratio at each station has been subtracted. At RTA, located in the South Pacific, a strong positive N_2O gradient of approximately 0.8 ppb (0 to 6000 m) is observed in June – August, as well as in the annual mean, while no significant gradient is observed in December – February. A similar feature is also seen in the SF_6 profiles at this site (not shown). The seasonal change in gradient corresponds with the north-south oscillation of the inter-tropical convergence zone (ITCZ). In the NH summer the ITCZ lies north of the Equator, thus air from the NH tropics, which has a higher N_2O mixing ratio, is mixed into the southern Hadley cell and descends in the SH sub-tropics. Only the two CTM models and TOMCAT approximately capture the strength of the gradient but in TOMCAT, the maximum mixing ratio occurs at too low altitude. The other models (MOZART4, TM5, TM3-NCEP, TM3-ERA, and LMDZ4) all underestimate the June – August and annual mean gradients to varying degrees. This appears not to be simply related to the Inter-Hemispheric (IH) exchange time, as TM5 has a long IH exchange time, while in LMDZ4 it is relatively short and in MOZART4 it is close to that observed (Patra et al., 2011). At HAA, located in the North Pacific, the air column above the PBL is very well mixed owing to the absence of strong local sources and to vigorous vertical mixing. All models are able to reproduce the observed vertical profile at this site. ULB is a mid-latitude station in central Mongolia. A negative vertical gradient is observed in all seasons, except autumn when it is positive, and has an annual mean value of approximately 0.4 ppb (from 1500 to 4000 m). The gradient is underestimated by all models (with the exception of TOMCAT in June – August) suggesting that either the emissions are underestimated in central Asia or that the modelled vertical mixing for this region is too strong. Although we cannot rule out the first possibility, the latter is consistent with previous studies, which found a systematic over-estimate of vertical mixing in the troposphere in northern mid-latitudes by CTMs (e.g. Stephens et al., 2007). At the high northern latitude site, PFA in Alaska, weak negative gradients are observed, approximately

0.2 ppb (1000 to 6000 m) for the annual mean. The gradient becomes stronger in December – February above 5000 m owing to the descent of N_2O-poor air from the lower stratosphere. At this site, the shape and strength of the gradient is fairly well reproduced by all models, a feature which is discussed further in section 3.3.1 in relation to the N_2O seasonal cycle in the high northern latitudes.

3.2.2. Meridional gradients

Meridional gradients and IH differences are some of the most commonly used constraints on tropospheric transport (Gloor et al., 2007; Patra et al., 2011). Patra et al. (2011) showed that most state-of-the-art transport models agree closely in the IH gradient of SF_6 (for which the emissions are fairly well known) as well as in the IH exchange rate. This study similarly finds good agreement with the observed SF_6 IH difference for all models that provided SF_6 simulations; however, the agreement is much poorer for N_2O (Fig. 5 and 6). Here the IH difference is calculated as the difference between the mean of all mixing ratios at background sites between 20°S - 90°S and 20°N - 90°N. All transport models underestimate the N_2O IH difference, regardless of which prior flux scenario is used (Table 8 and Fig. S3). The scenario BWMN04 results in the lowest IH differences for all models, while differences among the "OCN" scenarios are small and not consistent for all models. Considering the good agreement, or in some cases even overestimate, for SF_6, the poor agreement in the IH difference for N_2O is likely due to an inaccurate distribution of emissions between the NH and SH and/or too strong stratosphere to troposphere transport (STT) in the NH relative to the SH. The ocean N_2O flux estimates from Nevison et al. (1995; 2004) have been shown to overestimate the net ocean-atmosphere flux in the Southern Ocean (Hirsch et al., 2006; Huang et al., 2008) but this overestimate alone is not sufficient to explain the model-observation mismatch in the IH difference. Approximately, a difference of 6.5 TgN between the NH and SH emissions is needed to explain the observed IH mixing ratio difference of 1.44 ppb. With all models underestimating the observed gradient by at least 0.33 ppb (23%), which is equivalent to a mass of approximately 1.5 TgN, and assuming the overestimate of the Southern Ocean emissions to be approximately 1.0 TgN (Hirsch et al., 2006) leaves an unexplained north-south difference of 0.5 TgN. This could be due to errors in STT in the NH or it could be that there is still a bias in NH versus SH emissions, which could be corrected by a combination of reducing SH emissions and increasing NH emissions. The distribution of emissions within each hemisphere also influences how well each model captures the meridional gradient. The interplay between emissions and transport errors in each model explains why the models do

not all respond in the same way to the different flux scenarios, with respect to the IH difference and meridional gradient.

3.3. Factors determining the seasonality of N_2O

The seasonality of N_2O is determined by a combination of STT, tropospheric transport and surface fluxes (Ishijima et al., 2010). However, the importance of each of these determinants, and how this changes with latitude, remains uncertain. Nevison et al. (2007; 2011) have demonstrated the importance of seasonality in STT for the N_2O seasonal cycle in the troposphere but this mechanism appears to be less important in mid to low latitudes where seasonality in the surface fluxes are significant (Ishijima et al., 2010). We examine the varying influences on the tropospheric N_2O seasonal cycle focusing on seven sites, which cover a wide range of latitudes: BRW, MHD, THD, MLO, SMO, CGO, and SPO (see Table 4). While most are background sites, MHD, CGO, and THD are affected by local to regional-scale fluxes. MHD is periodically influenced by transport from the European continent (Biraud et al., 2002; Manning et al., 2011) and CGO is occasionally influenced by transport from southeastern Australia (Wilson et al., 1997). THD is affected by transport from the North American continent and, in the case of N_2O, by N_2O emissions from upwelling along the Californian coast (Lueker et al., 2003). THD is also a difficult site to model owing to the strong land/sea breeze cycle. Although this is not reproduced in global models, we expect the error in the simulated N_2O due to transport to be considerably smaller than for CO_2 since there is no significant diurnal cycle in N_2O fluxes, thus there is no diurnal rectifying effect.

Only ACTMt42l67, TM3-ERA, LMDZ4 and TOMCAT participated in the CFC-12 and SF_6 inter-comparisons, thus we have results for all three species from only these four models. The results of the inter-comparisons are presented in the following sections.

3.3.1. Influence of STT and tropospheric transport

To examine the influence of STT on the tropospheric seasonal cycle, we compare with CFC-12 because, like N_2O, the CFC-12 seasonal cycle is strongly influenced by STT (Liang et al., 2009; Nevison et al., 2007) but, unlike N_2O, the seasonality in the surface fluxes is likely to be only very small. The phase of the modelled seasonal cycle, i.e. the month of the minimum, for CFC-12 (upper panel) and N_2O (lower panel) is shown as a function of latitude and pressure in Figure 7. In all models, the NH CFC-12 and N_2O minima develop in the lower stratosphere and upper troposphere in winter and reach the lower troposphere in May – June

in the low to mid latitudes and in July – August in the high latitudes (TM3-NCEP is an exception as the minima occur about 1 month earlier compared to the other models). In the SH, the modelled minima develop in the lower stratosphere and upper troposphere in the austral spring to early summer, following the breakup of the polar vortex (except in TM3-NCEP where it is circa 2 months later). There is a lag of circa 1 to 3 months for the minima to reach the lower troposphere, where it occurs between January – April. We first examine the modelled seasonality in the lower troposphere by comparing with observations of N_2O, CFC-12 and SF_6 from the AGAGE and NOAA surface networks, and second, examine the N_2O seasonality at altitude by comparing with observations from NOAA flight profiles. Figure 8 shows the mean seasonal cycle (2006 – 2009) in N_2O, CFC-12 and SF_6 at AGAGE and NOAA surface sites. The seasonal cycle amplitudes have been normalized by the mean tropospheric abundance of each species to simplify the comparison between them.

3.3.1.1 Northern hemisphere

In the mid to high northern latitudes, a minimum in N_2O and CFC-12 is observed on average in August but for N_2O the timing varies from July to September depending on the year. At BRW and MHD, a considerable phase shift in the modelled N_2O seasonal cycle can be seen with respect to the observations, with the modelled minimum occurring between 2 and 4 months too early (Fig. 8). For CFC-12, however, the modelled seasonality coincides with the observations at MHD and is only circa 1 month too early at BRW (one exception is TM3-ERA at MHD, which has no clear seasonal cycle). The good agreement for CFC-12 for most models indicates that transport of air from the lower stratosphere into the troposphere in the high northern latitudes is adequately represented and, therefore, suggests that the model-observation phase shift in N_2O at these two sites is at least in part due to incorrect seasonality in emissions in the northern mid to high latitudes (this will be discussed further in section 3.3.2). At THD the observed and modelled seasonality in CFC-12 closely resembles that at MHD and BRW, whereas for N_2O the seasonality observed at THD has only circa half the amplitude and the phase is quite different with respect MHD and BRW. This points to a significant influence of N_2O surface fluxes on the observed seasonal cycle at this site, as also found by Nevison et al. (2011), and is most likely out-of-phase with the STT influence (also discussed further in section 3.3.2). In the tropics, at MLO, the observed seasonality in N_2O and CFC-12 has the same phase but only circa quarter of the amplitude of that seen at BRW while the modelled N_2O cycle, in contrast, has approximately the same amplitude as at BRW. The overestimate in the amplitude of the modelled seasonal cycle at MLO is most likely due

to an overestimate of the influence of STT at this site (as indicated by the timing of the minimum, i.e. in May, consistent with the modelled maximum in STT and a 3-month lag from crossing the tropopause to the lower troposphere) and to the problem in the seasonality of emissions in the northern mid to high latitudes (see section 3.3.2).

From the comparison of the observed seasonal cycles in the NH, a small shift to later CFC-12 and N_2O minima with increasing latitude was found (see Table 9) (THD is an exception as the N_2O seasonal cycle is strongly influenced by local land and ocean fluxes). The shift to later minimum with increasing latitude is also reproduced by most of the models (Fig. 7) and is consistent with the current understanding of STT. Air masses from the lower stratosphere are more strongly mixed into the troposphere in the extra-tropics where the transport can occur adiabatically along isentropes intersecting the tropopause (James et al., 2003; Stohl et al., 2003). Furthermore, once air masses cross the tropopause, they can be rapidly transported to the lower troposphere in the downward branch of the Hadley cell around 30°N (James et al., 2003). Therefore, the minimum is observed earlier in the mid latitudes than in the high latitudes where the rate of vertical transport is slower. Stratospheric air masses are then transported with the mean tropospheric meridional circulation towards higher latitudes. Considering this, the small phase shift in modelled CFC-12 (and part of the N_2O phase shift) compared with the observations at BRW may in fact be due to too rapid transport within the troposphere rather than too rapid or too early mixing across the tropopause.

3.3.1.2 Southern hemisphere

In SH high-latitudes, the observed N_2O and CFC-12 seasonal cycles differ significantly to those of the NH (i.e. they are not 6 months out-of-phase). Most models predict the minima at SPO in January – February, i.e. too early by circa 2 months (ACTMt42l32 is an exception where the N_2O minimum is about 2 months too late). However, for SF_6, the models match the observed cycle reasonably well at CGO and SPO. This can be understood in that the SF_6 seasonal cycle in the SH is largely due to seasonality in IH exchange and the strong meridional gradient in the atmosphere (Denning et al., 1999; Prinn et al., 2000), which is satisfactorily represented in the models. On the other hand, the N_2O and CFC-12 seasonal cycles are strongly modulated by STT and, in the case of N_2O, weakly modulated by ocean fluxes. The importance of STT has been shown previously at CGO using measurements of CFC-11 and CFC-12 (Nevison et al. 2005) and $\delta^{18}O$ and $\delta^{15}N$ isotopes in N_2O (Park et al., 2012). The model-observation mismatch for N_2O and CFC-12 points to a deficiency in

modelling STT in the SH. However, it is not easy to explain why the maximum influence of STT (resulting in a minimum in N_2O and CFC-12) is seen in April – May, which is 2 to 3 months later than one would expect given the winter (May to August) maximum in diabatic STT, the spring increase in tropopause height, and the spring breakup of the polar vortex, and points to gaps in our knowledge about STT in the SH. The observed seasonal cycles of N_2O and CFC-12 at SMO are closely in phase with that of SF_6, which can be explained in terms of IH transport and the north-south mixing ratio gradient and is consistent with previous studies (Nevison et al., 2007).

3.3.1.3 Altitude changes

To further investigate the influence of STT, we compare the modelled seasonal cycles at 4 different altitude ranges, from the lower troposphere to the tropopause, with NOAA aircraft data (unfortunately there is insufficient data coverage at RTA to be able to compare the seasonal cycles at this site). Figure 9 shows the observed and modelled N_2O as monthly means with the growth rate subtracted (as given in Table 7). At PFA, the influence of STT is seen between 6000 and 10000 m with an observed minimum occurring in late June. The timing of this minimum appears to be inconsistent with a winter maximum in diabatic STT due to the Brewer Dobson Circulation. However, as pointed out by Schoeberl (2004), most of the mass-exchange between the lower stratosphere and troposphere can be related to changes in the tropopause height with the maximum mass transfer to the troposphere occurring in spring as the tropopause height is increasing. In which case, allowing for the lag time for vertical and horizontal transport within the troposphere of approximately 2 months according to Liang et al. (2009), a June minimum is not unexpected. Another consideration for the timing of the minimum is the seasonal cycle of N_2O in the stratosphere itself, which must be convolved with that of STT to explain the influence on tropospheric seasonality (Liang et al., 2009). Since N_2O is destroyed photochemically, extra-tropical stratospheric loss of N_2O has a maximum in summer and minimum in winter, thus the phase of the seasonal cycle in the stratosphere will lead to a later minimum in the troposphere (as compared to no seasonality in the stratosphere). Below 6000 m, the minimum occurs significantly later again, in August. The reason for the August minimum is likely twofold: 1) owing to the time needed to transport the STT influence in the mid latitudes (where most STT occurs) to the high northern latitudes and 2) owing to the increase in PBL height, which means the fluxes are mixed into a greater volume of air, thereby decreasing the mixing ratio. Although all models predict a too early minimum above 6000 m (by circa 2.5 months), the phase shift between the modelled

and observed minima is fairly constant across all altitudes, consistent with the finding that the modelled vertical gradient at this site agrees with observations (see Fig. 4).

At ULB, the influence of STT can be seen between 4000 and 6000 m with a minimum in July but the amplitude of the cycle decreases at lower altitudes suggesting a weaker influence of STT in the lower troposphere at this latitude. Although the phase of the cycle in the 4000 – 6000 m altitude range is fairly closely captured by most models, they overestimate its amplitude below 4000 m. Lastly, at HAA, the observed seasonal cycle is consistent in amplitude and phase from 500 to 6000 m, owing to vigorous vertical mixing. However, all models predict a too early minimum below 6000 m and overestimate the amplitude suggesting that the modelled influence of STT at this latitude is too strong.

3.3.2. Influence of surface fluxes

The influence of changing the surface fluxes of N_2O on the seasonal cycle in the lower troposphere was investigated by performing four different transport model integrations with each of the four prior flux estimates: OCNPIC, OCNN95, OCNN04 and BWMN04 (see Tables 2 and 3 for details and Fig. S4 for Hovmöller plots of the flux components). Figure 10 compares the observed and modelled seasonal cycles at each site (BRW, MHD, THD, MLO, SMO, and CGO) as a separate panel, and the four subplots within each panel are for each of the four flux scenarios. Also shown within each subplot, is the area weighted mean N_2O flux for an area of 10° × 30° (latitude by longitude) centred on the site. At BRW, the best match to the observed cycle was provided by the BWMN04 fluxes while the other three (all using OCN terrestrial biosphere fluxes) were very similar in phase and amplitude. Around the site itself, the flux is very low and there is little difference between the BWM and OCN terrestrial fluxes (the flux difference is solely due to the choice of ocean flux estimate). The improved fit to the seasonal cycle in the mixing ratio at BRW, therefore, must result from the difference between OCN and BWM in the mid northern latitudes; OCN predicts a late summer maximum while there is no seasonal cycle in BWM. The phase modelled with BWMN04 matches almost exactly (correlation coefficient $R^2 \geq 0.95$) for all models except TM3-NCEP. Furthermore, considering that for CFC-12 at this site has a phase shift of only approximately 1 month, the mismatch in the OCN simulations is unlikely to be from transport model errors. Similarly at MHD, BWMN04 provides the best fit to the observations ($R^2 \geq 0.79$, except TM3-NCEP). These results show that the inclusion of a seasonal cycle in the OCN terrestrial fluxes does not improve the fit to the observations but rather makes it worse, indicating that

the seasonality, in particular the late summer maximum, in OCN is not realistic. From what is known about the processes driving the terrestrial biosphere N_2O flux, higher emissions are expected during the growing season owing to warmer soil temperatures leading to increased microbial activity and higher reactive nitrogen turnover rates. However, OCN most likely overestimates the late summer emissions while underestimating the emissions in spring and early summer. This is due to the lack of a vertically resolved soil-layer, which prevents the realistic simulation of the impact of rain events and tends to predict anoxic soil conditions, necessary for N_2O production via denitrification, predominantly in summer rather than distributed throughout the year as would be more realistic (personal communication, S. Zaehle, 2012). This result highlights the complexity of modelling terrestrial ecosystem N_2O fluxes and the need for independent validation. Again at THD, BWMN04 gives the closest fit to the observed seasonal cycle matching the amplitude but still resulting in a too early minimum by circa 3 months. Since THD is also strongly influenced by N_2O emissions from upwelling along the Californian coast (Lueker et al., 2003), this model-observation mismatch may also indicate deficiencies in the coastal N_2O fluxes.

At MLO, the regional flux differences are due to differences between the ocean flux models, PIC, N95 and N04. However, an improvement in the modelled seasonal cycle in N_2O mixing ratio only occurs when the BWM terrestrial fluxes are used ($R^2 \geq 0.27$, except TM3-NCEP, compared with no correlation with the other fluxes). This shows that the seasonality at MLO is also influenced by NH terrestrial fluxes as has also been previously shown (Patra et al., 2005). For SMO, the modelled seasonality is very similar for all flux models (N04 results in a small phase shift to a later minimum), which can be understood in that this site is strongly affected by IH exchange rather than the seasonality of surface fluxes in this latitude. In the southern mid-latitudes, at CGO, OCNPIC and OCNN95 give the best agreement to the observed seasonal cycle. Replacing the terrestrial biosphere fluxes, OCN, with BWM made no significant difference, as expected since this site is only very weakly influenced by land fluxes. For SPO, changing the fluxes had negligible influence on the modelled mixing ratios (this site is not shown), highlighting again the importance of STT at this site.

4. Summary and Conclusions

This TransCom study has investigated the influence of emissions, tropospheric transport and Stratosphere-Troposphere Exchange (STE) on the variability in atmospheric N_2O, focusing on seasonal to annual time-scales. In particular, our aim has been to examine the influence of

errors in atmospheric transport versus errors in prior fluxes on modelled mixing ratios by comparing simulated mixing ratios with atmospheric observations of N_2O as well as CFC-12 to assess the ability of models to reproduce STE and, additionally, of SF_6 to assess the tropospheric transport in the models. Knowledge about prior flux and transport errors has important implications for the set-up of inverse models for estimating N_2O surface emissions and for the interpretation of their results. In total, six different transport models and two model variants were included in this inter-comparison.

To assess the representation of global-scale transport and, in particular, inter-hemispheric transport, we compared the modelled and observed IH gradients of N_2O and SF_6. We found good agreement between the modelled and observed south to north gradient and IH difference for SF_6 in line with previous studies (e.g. Patra et al., 2011), which indicates that the models adequately capture the rate of IH mixing as well as mixing between tropical and extra-tropical regions. For N_2O, however, the IH difference was underestimated compared to the observations in all models by at least 0.33 ppb, equivalent to approximately 1.5 TgN. Assuming that emissions in the Southern Ocean are overestimated by approximately 1.0 TgN (Hirsch et al., 2006) leaves an unexplained north-south difference of 0.5 TgN. This most likely indicates a larger NH to SH source ratio than prescribed in the prior emissions but an over-estimate of the influence of STT in the NH may also still contribute to the model-observation difference in the IH gradient.

Using a combination of aircraft profiles (NOAA flights) and surface sites (NOAA and AGAGE networks), we have compared the modelled and observed N_2O seasonal cycles from the surface to the upper troposphere and the CFC-12 and SF_6 seasonal cycles at the surface. We found that all models that simulated CFC-12 accurately matched the phase and amplitude of the CFC-12 cycle at MHD and were only circa 1 month out-of-phase at BRW. In contrast, modelled N_2O seasonal cycles were all 2-3 months out-of-phase at both sites. The model – observation mismatch in the N_2O seasonal cycle at NH sites is, thus, likely not to be due to errors in atmospheric transport, which on the basis of the CFC-12 comparison are in the order of the measurement precision (i.e. 0.1 ppb), but rather due to errors in the N_2O flux. Additionally, when the simulations using the BWM terrestrial ecosystem fluxes (as opposed to OCN) were compared, a much better agreement with the observations was found for BRW, MHD, THD and MLO. While the BWM fluxes have no seasonal component, OCN predicts a late summer maximum. Even after considering the seasonality of STT, a late summer

maximum in the surface N_2O fluxes in the mid to high northern latitudes is inconsistent with observations. Late summer emissions are likely overestimated in OCN, while emissions in spring and autumn are likely underestimated. Furthermore, the timing of the N_2O mixing ratio minimum in the upper troposphere in the extra-tropical northern latitudes (in June – July) occurs too late to be predominantly due to the winter maximum in diabatic STT i.e., driven by the Brewer Dobson circulation as previously suggested (Nevison et al. 2007; Nevison et al. 2011) but rather is consistent with the effect of increasing tropopause height in spring (Schoeberl, 2004). This spring maximum in mass transfer, convoluted with the seasonality of N_2O loss in the stratosphere and the lag time for this signal to be transported in the troposphere (circa 2 months) more likely explains the phase of the observed signal.

In the southern low latitudes, at SMO, the influence is mostly from IH transport as previously found for SF_6 (Denning et al., 1999; Prinn et al., 2000) and N_2O (Nevison et al., 2007; Nevison et al., 2011). While in the SH mid to high latitudes, CGO and SPO are strongly influenced by STT and weakly influenced by meridional transport and ocean surface fluxes, as previously shown (Park et al., 2012). The error at these sites due to transport is significant for all models, and thus will result in errors in the seasonality and, with seasonal dependence of atmospheric transport, in the location of emissions estimated from atmospheric inversions.

To conclude, the comparison of modelled and observed N_2O mixing ratios has been shown to provide important constraints on the broad spatial distribution of N_2O emissions and, in the NH, on their seasonality. However, modelled N_2O mixing ratios are sensitive to non-random model transport errors, particularly, in the magnitude of STT, which will contribute to errors in N_2O emissions estimates from atmospheric inversions. In the SH mid to high latitudes, the influence of transport errors on modelled N_2O mixing ratios is even more important, again largely due to errors in STT, and means that current estimates of seasonality and, to some extent, the location of N_2O emissions in the SH from atmospheric inversions may not be reliable.

Acknowledgments

We would like to thank C. Nevison, S. Zaehle, L. Bouwman, L. Bopp, and G. van der Werf for providing their N_2O emissions estimates. We also thank F. Chevallier and S. Zaehle for their comments, which improved this manuscript. Additionally, we would like to

acknowledge everyone who contributed to the measurements of N_2O without which we would not have been able to make this inter-comparison study.

References

Aumont, O. and Bopp, L.: Globalizing results from ocean in situ iron fertilization studies. Global Biogeochem. Cycles, 20, GB2017, doi:10.1029/2005gb002591, 2006

Biraud, S., Ciais, P., Ramonet, M., Simmonds, P., Kazan, V., Monfray, P., O'Doherty, S., Spain, G. and Jennings, S. G.: Quantification of carbon dioxide, methane, nitrous oxide and chloroform emissions over Ireland from atmospheric observations at Mace Head, Tellus, 54B, 41 - 60, 2002.

Bouwman, A. F., Boumans, L. J. M. and Batjes, N. H.: Modeling global annual N_2O and NO emissions from fertilized fields. Global Biogeochem. Cy., 16, (4), 1080, doi: 10.1029/2001GB001812, 2002

Butler, J. H. (2011). "The NOAA Annual Greenhouse Gas Index." from http://www.esrl.noaa.gov/gmd/aggi/.

Chipperfield, M. P.: New version of the TOMCAT/SLIMCAT off-line chemical transport model: Intercomparison of stratospheric tracer experiments, Q. J. R. Meteorol. Soc., 132, 1179-1203, 2006.

Corazza, M., Bergamaschi, P., Vermeulen, A. T., Aalto, T., Haszpra, L., Meinhardt, F., O'Doherty, S., Thompson, R., Moncrieff, J., Popa, E., Steinbacher, M., Jordan, A., Dlugokencky, E., Brühl, C., Krol, M. and Dentener, F.: Inverse modelling of European N2O emissions: assimilating observations from different networks, Atmos. Chem. Phys., 11 (5), 2381-2398, 2011.

Denning, A. S., Holzer, M., Gurney, K. R., Heimann, M., Law, R. M., Rayner, P. J., Fung, I. Y., Fan, S.-M., Taguchi, S., Freidlingstein, P., Balkanski, Y., Taylor, J., Maiss, M. and Levin, I.: Three-dimensional transport and concentration of SF_6: A model intercomparison study (TransCom 2), Tellus, 51B, 266-297, 1999.

Emmons, L. K., Walters, S., Hess, P. G., Lamarque, J.-F., Pfister, G. G., Fillmore, D., Granier, C., Guenther, A., Kinnison, D., Laepple, T., Orlando, J., Tie, X., Tyndall, G., Wiedinmyer, C., Baughcum, S. L. and Kloster, S.: Description and evaluation of the Model for Ozone and Related chemical Tracers, version 4 (MOZART-4), Geosci. Model Dev., 3, 43-67, 2010.

Forster, P., Ramaswamy, V., Artaxo, P., Berntsen, T., Betts, R., Fahey, D. W., Haywood, J., Lean, J., Lowe, D. C., Myhre, G., Nganga, J., Prinn, R., Raga, G., Schultz, M. and Van

Dorland, R.: Changes in Atmospheric Constituents and in Radiative Forcing, Climate Change 2007: The Physical Science Basis. Contribution of Working Group I to the Fourth Assessment Report of the Intergovernmental Panel on Climate Change. Solomon, S., Qin, D., Manning, M., Chen, Z., Marquis, M., Averyt, K. B., Tignor, M. and Miller, H. L., Cambridge University Press. Cambridge, United Kingdom. 2007.

Galloway, J. N., Townsend, A. R., Erisman, J. W., Bekunda, M., Cai, Z., Freney, J. R., Martinelli, L. A., Seitzinger, S. P. and Sutton, M. A.: Transformation of the Nitrogen Cycle: Recent Trends, Questions, and Potential Solutions, Science, 320 (5878), 889-892, 2008.

Geels, C., Gloor, M., Ciais, P., Bousquet, P., Peylin, P., Vermeulen, A. T., Dargaville, R., Aalto, T., Brandt, J., Christensen, J. H., Frohn, L. M., Haszpra, L., Karstens, U., Rodenbeck, C., Ramonet, M., Carboni, G. and Santaguida, R.: Comparing atmospheric transport models for future regional inversions over Europe - Part 1: mapping the atmospheric CO_2 signals, Atmos. Chem. Phys., 7, 3461-3479, 2007.

Gloor, M., Dlugokencky, E., Brenninkmeijer, C., Horowitz, L., Hurst, D. F., Dutton, G., Crevoisier, C., Machida, T. and Tans, P.: Three-dimensional SF_6 data and tropospheric transport simulations: Signals, modeling accuracy, and implications for inverse modeling, J. Geophys. Res., 112, D15112, doi:10.1029/2006JD007973, 2007.

Hall, B. D., Dutton, G. S. and Elkins, J. W.: The NOAA nitrous oxide standard scale for atmospheric observations. J. Geophys. Res., 112, D09305, doi: 10.1029/2006jd007954, 2007

Heimann, M. and Körner, S.: The global atmospheric tracer model TM3. Technical Report 5. Jena, Germany, Max Planck Institute for Biogeochemistry, 2003.

Hirsch, A. I., Michalak, A. M., Bruhwiler, L. M., Peters, W., Dlugokencky, E. J. and Tans, P. P.: Inverse modeling estimates of the global nitrous oxide surface flux from 1998-2001. Global Biogeochem. Cy., 20, GB1008, doi:10.1029/2004GB002443, 2006

Holton, J. R., Haynes, P. H., McIntyre, M. E., Douglass, A. R., Rood, R. B. and Pfister, L.: Stratosphere-troposphere exchange, Rev. Geophys., 33 (4), 403-439, 1995.

Hourdin, F., Musat, I., Bony, S., Braconnot, P., Codron, F., Dufresne, J.-L., Fairhead, L., Filiberti, M.-A., Friedlingstein, P., Grandpeix, J.-Y., Krinner, G., Le Van, P., Li, Z.-X. and Lott, F.: The LMDZ4 general circulation model: climate performance and sensitivity to parameterized physics with emphasis on tropical convection, Clim. Dyn., 27, 787-813, 2006.

Huang, J., Golombek, A., Prinn, R., Weiss, R., Fraser, P., Simmonds, P., Dlugokencky, E. J., Hall, B., Elkins, J., Steele, P., Langenfelds, R., Krummel, P., Dutton, P. and Porter, L.: Estimation of regional emissions of nitrous oxide from 1997 to 2005 using multinetwork measurements, a chemical transport model, and an inverse method. J. Geophys. Res., 113, (D17313), doi:10.1029/2007JD009381, 2008

Ishijima, K., Patra, P. K., Takigawa, M., Machida, T., Matsueda, H., Sawa, Y., Steele, L. P., Krummel, P. B., Langenfelds, R. L., Aoki, S. and Nakazawa, T.: Stratospheric influence on the seasonal cycle of nitrous oxide in the tropospheric as deduced from aircraft observations and model simulations. J. Geophys. Res., 115, (D20308), doi:10.1029/2009JD013322, 2010

James, P., Stohl, A., Forster, C., Eckhardt, S., Seibert, P. and Frank, A.: A 15-year climatology of stratosphere - troposphere exchange with a Lagrangian particle dispersion model 2. Mean climate and seasonal variability, J. Geophys. Res., 108 (D12), 8522, doi:10.1029/2002JD002639, 2003.

Law, R. M., Peters, W., Rödenbeck, C., Aulagnier, C., Baker, I., Bergmann, D. J., Bousquet, P., Brandt, J., Bruhwiler, L., Cameron-Smith, P. J., Christensen, J. H., Delage, F., Denning, A. S., Fan, S., Geels, C., Houweling, S., Imasu, R., Karstens, U., Kawa, S. R., Kleist, J., Krol, M. C., Lin, S. J., Lokupitiya, R., Maki, T., Maksyutov, S., Niwa, Y., Onishi, R., Parazoo, N., Patra, P. K., Pieterse, G., Rivier, L., Satoh, M., Serrar, S., Taguchi, S., Takigawa, M., Vautard, R., Vermeulen, A. T. and Zhu, Z.: TransCom model simulations of hourly atmospheric CO_2: Experimental overview and diurnal cycle results for 2002, Global Biogeochem. Cycles, 22 (3), GB3009, doi: 10.1029/2007gb003050, 2008.

Law, R. M., Rayner, P. J., Denning, A. S., Erickson, D., Fung, I. Y., Heimann, M., Piper, S. C., Ramonet, M., Taguchi, S., Taylor, J. A., Trudinger, C. M. and Watterson, I. G.: Variations in modelled atmospheric transport of carbon dioxide and the consequences for CO2 inversions, Global Biogeochem. Cycles, 10 (4), 783-796, 1996.

Levin, I., Naegler, T., Heinz, R., Osusko, D., Cuevas, E., Engel, A., Ilmberger, J., Langenfelds, R. L., Neininger, B., Rohden, C. v., Steele, L. P., Weller, R., Worthy, D. E. and Zimov, S. A.: The global SF_6 source inferred from long-term high precision atmospheric measurements and its comparison with emission inventories, Atmos. Chem. Phys., 10 (6), 2655-2662, 2010.

Liang, Q., Douglass, A. R., Duncan, B. N., Stolarski, R. S. and Witte, J. C.: The governing processes and timescales of stratosphere-to-troposphere transport and its contribution to ozone in the Arctic troposphere, Atmos. Chem. Phys., 9 (9), 3011-3025, 2009.

Lueker, T. J., Walker, S. J., Vollmer, M. K., Keeling, R. F., Nevison, C. D. and Weiss, R. F.: Coastal upwelling air-sea fluxes revealed in atmospheric observations of O_2/N_2, CO_2 and N_2O, Geophysical Research Letters, 30 (6), 1292-1295, 2003.

Manning, A. J., O'Doherty, S., Jones, A. R., Simmonds, P. G. and Derwent, R. G.: Estimating UK methane and nitrous oxide emissions from 1990 to 2007 using an inversion modeling approach, J. Geophys. Res., 116 (D2), D02305, doi: 10.1029/2010jd014763, 2011.

McCulloch, A., Midgley, P. M. and Ashford, P.: Releases of refrigerant gases (CFC-12, HCFC-22 and HFC-134a) to the atmosphere, Atmospheric Environment, 37 (7), 889-902, 2003.

Minschwaner, K., Salawitch, R. J. and McElroy, M. B.: Absorption of Solar Radiation by O_2: Implications for O_3 and Lifetimes of N_2O, $CFCl_3$, and CF_2Cl_2, J. Geophys. Res., 98 (D6), 10,543-510,561, 1993.

Morris, R. A., Viggiano, A. A., Arnold, S. T. and Paulson, J. F.: Chemistry of atmospheric ions reacting with fully fluorinated compounds, International Journal of Mass Spectrometry and Ion Processes, 149-150 (0), 287-298, 1995.

Nevison, C. D., Dlugokencky, E., Dutton, G., Elkins, J. W., Fraser, P., Hall, B., Krummel, P. B., Langenfelds, R. L., O'Doherty, S., Prinn, R. G., Steele, L. P. and Weiss, R. F.: Exploring causes of interannual variability in the seasonal cycles of tropospheric nitrous oxide, Atmos. Chem. Phys., 11 (8), 3713-3730, 2011.

Nevison, C. D., Keeling, R. F., Weiss, R. F., Popp, B. N., Jin, X., Fraser, P. J., Porter, L. W. and Hess, P. G.: Southern Ocean ventilation inferred from seasonal cycles of atmospheric N_2O and O_2/N_2 at Cape Grim, Tasmania, Tellus B, 57 (3), 218-229, 2005.

Nevison, C. D., Lueker, T. J. and Weiss, R. F.: Quantifying the nitrous oxide source from coastal upwelling. Global Biogeochem. Cycles, 18, GB1018, doi:10.1029/2003GB002110, 2004

Nevison, C. D., Mahowald, N. M., Weiss, R. F. and Prinn, R. G.: Interannual and seasonal variability in atmospheric N_2O. Global Biogeochem. Cycles, 21, GB3017, doi: 10.1029/2006gb002755, 2007

Nevison, C. D., Weiss, R. F. and Erickson, D. J.: Global oceanic emission of nitrous oxide, J. Geophys. Res., 100, 15809-15820, 1995.

Park, S., Croteau, P., Boering, K. A., Etheridge, D. M., Ferretti, D., Fraser, P. J., Kim, K. R., Krummel, P. B., Langenfelds, R. L., van Ommen, T. D., Steele, L. P. and Trudinger, C. M.: Trends and seasonal cycles in the isotopic composition of nitrous oxide since 1940, Nature Geosci, 5 (4), 261-265, 2012.

Patra, P. K., Houweling, S., Krol, M., Bousquet, P., Belikov, D., Bergmann, D., Bian, H., Cameron-Smith, P., Chipperfield, M. P., Corbin, K., Fortems-Cheiney, A., Fraser, A., Gloor, E., Hess, P., Ito, A., Kawa, S. R., Law, R. M., Loh, Z., Maksyutov, S., Meng, L., Palmer, P. I., Prinn, R. G., Rigby, M., Saito, R. and Wilson, C.: TransCom model simulations of CH4 and related species: linking transport, surface flux and chemical loss with CH_4 variability in the troposphere and lower stratosphere, Atmos. Chem. Phys., 11 (24), 12813-12837, 2011.

Patra, P. K., Maksyutov, S. and Nakazawa, T.: Analysis of atmospheric CO_2 growth rates at Mauna Loa using CO_2 fluxes derived from an inverse model, Tellus B, 57 (5), 357-365, 2005.

Patra, P. K., Takigawa, M., Dutton, G. S., Uhse, K., Ishijima, K., Lintner, B. R., Miyazaki, K. and Elkins, J. W.: Transport mechanisms for synoptic, seasonal and interannual SF_6 variations and "age" of air in troposphere, Atmos. Chem. Phys., 9 (4), 1209-1225, 2009.

Prather, M. J., Holmes, C. D. and Hsu, J.: Reactive greenhouse gas scenarios: Systematic exploration of uncertainties and the role of atmospheric chemistry, Geophys. Res. Lett., 39, L09803, doi:10.1029/2012GL051440, 2012.

Prinn, R. G., Weiss, R. F., Fraser, P. J., Simmonds, P. G., Cunnold, D. M., Alyea, F. N., O'Doherty, S., Salameh, P., Miller, B. R., Huang, J., Wang, R. H. J., Hartley, D. E., Harth, C., Steele, L. P., Sturrock, G., Midgley, P. M. and McCulloch, A.: A history of chemically and radiatively important gases in air deduced from ALE/GAGE/AGAGE, J. Geophys. Res., 105 (D14), 17751-17792, 2000.

Ravishankara, A. R., Daniel, J. S. and Portmann, R. W.: Nitrous Oxide (N_2O): The Dominant Ozone-Depleting Substance Emitted in the 21st Century, Science, 326 (5949), 123-125, 2009.

Ravishankara, A. R., Solomon, S., Turnipseed, A. A. and Warren, R. F.: Atmospheric Lifetimes of Long-Lived Halogenated Species, Science, 259 (5092), 194-199, 1993.

Reichler, T., Dameris, M. and Sausen, R.: Determining the tropopause height from gridded data, Geophys. Res. Lett., 30, 2042, doi:10.1029/2003GL018240, 2003.

Saikawa, E., Schlosser, C. A., and Prinn, R. G.: Global modeling of soil nitrous oxide emissions from natural processes, Global Biogeochem. Cycles, 27, 972-989, 2013.

Schoeberl, M. R.: Extratropical stratosphere-troposphere mass exchange. J. Geophys. Res. - Atmos., 109, D13303, doi:10.1029/2004jd004525, 2004

Seinfeld, J. H. and Pandis, S. N.: Atmospheric Chemistry and Physics: from Air Pollution to Climate Change, John Wiley and Sons, New York, USA, 1326pp, 1998.

Stephens, B. B., Gurney, K. R., Tans, P. P., Sweeney, C., Peters, W., Bruhwiler, L., Ciais, P., Ramonet, M., Bousquet, P., Nakazawa, T., Aoki, S., Machida, T., Inoue, G., Vinnichenko, N., Lloyd, J., Jordan, A., Heimann, M., Shibistova, O., Langenfelds, R. L., Steele, L. P., Francey, R. J. and Denning, A. S.: Weak Northern and Strong Tropical Land Carbon Uptake from Vertical Profiles of Atmospheric CO_2, Science, 316 (5832), 1732-1735, 2007.

Stohl, A., Bonasoni, P., Cristofanelli, P., Collins, W., Feichter, J., Frank, A., Forster, C., Gerasopoulos, E., Gaggeler, H., James, P., Kentarchos, T., Kromp-Kolb, H., Kruger, B., Land, C., Meloen, J., Papayannis, A., Priller, A., Seibert, P., Sprenger, M., Roelofs, G. J., Scheel, H. E., Schnabel, C., Siegmund, P., Tobler, L., Trickl, T., Wernli, H., Wirth, V., Zanis, P. and Zerefos, C.: Stratosphere-troposphere exchange: A review, and what we have learned from STACCATO, Journal of Geophysical Research-Atmospheres, 108 (D12), 8516, doi:10.1029/2002JD002490, 2003.

Thompson, R. L., Dlugockenky, E., Chevallier, F., Ciais, P., Dutton, G., Elkins, J. W., Langenfelds, R. L., Prinn, R. G., Weiss, R. F., Tohjima, Y., Krummel, P. B., Fraser, P. and Steele, L. P.: Interannual variability in tropospheric nitrous oxide, Geophys. Res. Lett., 40 (1-6), doi:10.1002/grl.50721, 2013.

Thompson, R. L., Chevallier, F., Crotwell, A. M., Dutton, G., Langenfelds, R. L., Prinn, R. G., Weiss, R. F., Tohjima, Y., Nakazawa, T., Krummel, P. B., Steele, L. P., Fraser, P., O'Doherty, S., Ishijima, K., and Aoki, S.: Nitrous oxide emissions 1999 to 2009 from a global atmospheric inversion, Atmos. Chem. Phys., 14, doi: 10.5194/acp-14-1801-2014, 2014a.

Thompson, R. L., Ishijima, K., Saikawa, E., Corazza, M., Karstens, U., Patra, P. K., Bergamaschi, P., Chevallier, F., Dlugokencky, E., Prinn, R. G., Weiss, R. F., O'Doherty, S., Fraser, P. J., Steele, L. P., Krummel, P. B., Vermeulen, A., Tohjima, Y., Jordan, A., Haszpra, L., Steinbacher, M., Van der Laan, S., Aalto, T., Meinhardt, F., Popa, M. E., Moncrieff, J., and P. Bousquet: TransCom N_2O model inter-comparison, Part II: Atmospheric inversion estimates of N_2O emissions, Atmos. Chem. Phys. Discuss., 14, doi:10.5194/acpd-14-5271-2014, 2014b.

Thompson, T. M., Elkins, J. W., Hall, B., Dutton, G. S., Swanson, T. H., Butler, J. H., Cummings, S. O. and Fisher, D. A.: Halocarbons and other Atmospheric Trace Species. Climate Diagnostics Laboratory Summary Report #27, 2002-2003. Boulder, Colorado, US Department of Commerce, National Oceanic and Atmospheric Administration, 2004.

van der Werf, G. R., Randerson, J. T., Giglio, L., Collatz, G. J., Mu, M., Kasibhatla, P. S., Morton, D. C., DeFries, R. S., Jin, Y. and van Leeuwen, T. T.: Global fire emissions and the contribution of deforestation, savanna, forest, agricultural, and peat fires (1997-2009), Atmos. Chem. Phys., 10 (23), 11707-11735, 2010.

Volk, C. M., Elkins, J. W., Fahey, D. W., Dutton, G. S., Gilligan, J. M., Loewenstein, M., Podolske, J. R., Chan, K. R. and Gunson, M. R.: Evaluation of source gas lifetimes from stratospheric observations, J. Geophys. Res., 102 (D21), 25,543-525,564, 1997.

Wilson, S. R., Dick, A. L., Fraser, P. J., and Whittlestone S.: Nitrous oxide flux estimates for southeastern Australia, J. Atmos. Chem., 26(2), 169-188, 1997.

WMO: Greenhouse Gas Bulletin: The State of Greenhouse Gases in the Atmosphere Based on Global Observations through 2010Atmospheric Environment Research Division, Research Department, World Meteorological Organisation, Geneva, 2011.

Zaehle, S. and Friend, A. D.: Carbon and nitrogen cycle dynamics in the O-CN land surface model: 1. Model description, site-scale evaluation, and sensitivity to parameter estimates. Global Biogeochem. Cycles, 24, GB1005, doi: 10.1029/2009gb003521, 2010

Table 1. Transport model overview

Model	Institution	Resolution Horizontal (lon × lat)	Vertical	Meteorology	Max Alt. (hPa)	
MOZART4[1]	MIT/Emory	2.5° × 1.88°	56 σ[8]	MERRA[10]	2	offline
ACTMt42l32[2]	RIGC	2.8° × 2.8°	32 σ	NCEP2[11]	3	online
ACTMt42l67[3]	RIGC	2.8° × 2.8°	67 σ	JRA25[12]	0.01	online
TM5[4]	JRC	6.0° × 4.0°	25 η[9]	ERA-interim[13]	0.5	offline
TM3-NCEP[5]	MPI-BGC	5.0° × 3.75°	19 η	NCEP	23	offline
TM3-ERA[5]	MPI-BGC	5.0° × 3.75°	26 η	ERA-interim	1	offline
LMDZ4[6]	LMD/LSCE	3.75° × 2.5°	19 η	ERA-interim	4	online
TOMCAT[7]	Univ. of Leeds	2.8° × 2.8°	60 η	ERA-interim	0.1	offline

1. (Emmons et al., 2010)
2. (Patra et al., 2009)
3. (Ishijima et al., 2010)
4. (Corazza et al., 2011)
5. (Heimann and Körner, 2003)
6. (Hourdin et al., 2006)
7. (Chipperfield, 2006)
8. σ refers to the sigma terrain-following vertical coordinate system
9. η refers to the eta coordinate system that smoothly transitions from the sigma coordinate near the surface to a pressure coordinate in the stratosphere
10. Modern ERa Retrospective Analysis for research and applications
11. National Centers for Environmental Protection
12. Japanese 25-year Reanalysis project
13. European Centre for Medium-range Weather Forecasting Reanalysis

Table 2. Overview of the reference prior fluxes (OCNPIC) (totals shown for 2005)

Category	Dataset	Resolution	Total (TgN y^{-1})
terrestrial biosphere	ORCHIDEE O-CN	monthly	10.83
ocean	PISCES	monthly	4.28
waste water	EDGAR-4.1	annual	0.21
solid waste	EDGAR-4.1	annual	0.004
solvents	EDGAR-4.1	annual	0.05
fuel production	EDGAR-4.1	annual	0.003
ground transport	EDGAR-4.1	annual	0.18
industry combustion	EDGAR-4.1	annual	0.41
residential & other combustion	EDGAR-4.1	annual	0.18
shipping	EDGAR-4.1	annual	0.002
other sources	EDGAR-4.1	annual	0.0005
biomass burning	GFED-2	monthly	0.71
Total		monthly	16.84

1 Table 3. Overview of the additional prior fluxes (totals shown for 2005)

Flux set	Categories	Dataset	Resolution	Total (TgN y^{-1})
OCNN95	terrestrial biosphere	ORCHIDEE OCN	monthly	10.83
	ocean	Nevison et al. 1995	monthly	3.59
	anthropogenic	EDGAR-4.1[a]	annual	1.04
	biomass burning	GFED-2	monthly	0.71
	total			16.17
OCNN04	terrestrial biosphere	ORCHIDEE OCN	monthly	10.83
	ocean	Nevison et al. 2004	monthly	4.44
	anthropogenic	EDGAR-4.1	annual	1.04
	biomass burning	GFED-2	monthly	0.71
	total			17.02
BWMN04	natural ecosystem	Bouwman et al. 2002	monthly	4.59
	ocean	Nevison et al. 2004	monthly	4.44
	anthropogenic and agriculture	EDGAR-4.1[b]	annual	4.54
	biomass burning	GFED-2	monthly	0.71
	total			14.28

2 a. EDGAR categories: 6B, 6A-6C, 3, 1B, 1A3bce, 1A2-2, 1A4-5, 1A3d, 7
3 b. EDGAR categories: 6B, 6A-6C, 3, 1B, 1A3bce, 1A2-2, 1A4-5, 1A3d, 7, 4
4
5
6

Table 4. Atmospheric sites used in the analysis

ID	Station	Network	Type	Latitude	Longitude	Altitude (masl)[#]
ALT	Alert	NOAA	F	82.5°N	62.5°W	210
ZEP	Ny-Alesund	NOAA	F	78.9°N	11.88°E	475
BRW	Barrow	NOAA	F, C*	71.3°N	156.6°W	11
MHD	Macehead	AGAGE	C, C*	53.3°N	9.9°W	25
		NOAA	F			
SHM	Shemya Island	NOAA	F	52.7°N	174.1°E	40
THD	Trinidad Head	AGAGE	C, C*	41.1°N	124.2°W	107
		NOAA	F			
NWR	Niwot Ridge	NOAA	F, C*	40.0°N	105.5°W	3526
IZO	Tenerife	NOAA	F	28.3°N	16.5°W	2360
KUM	Cape Kumukahi	NOAA	F	19.5°N	154.8°W	3
MLO	Mauna Loa	NOAA	F, C*	19.5°N	155.6°W	3397
RPB	Ragged Point	AGAGE	C, C*	13.2°N	59.4°W	45
		NOAA	F			
CHR	Christmas Island	NOAA	F	1.7°N	157.2°W	3
SEY	Seychelles	NOAA	F	4.7°S	55.2°E	3
ASC	Ascension Island	NOAA	F	7.9°S	14.4°W	54
SMO	Samoa	AGAGE	C, C*	14.3°S	170.6°W	42
		NOAA	F			
EIC	Easter Island	NOAA	F	27.2°S	109.5°W	50
CGO	Cape Grim	AGAGE	C, C*	40.7°S	144.7°E	164
		NOAA	F			
TDF	Tierra del Fuego	NOAA	F	54.9°S	68.5°W	20
HBA	Halley Station	NOAA	F	75.6°S	26.5°W	30
SPO	South Pole	NOAA	F, C*	89.98°S	24.8°W	2810
PFA	Poker Flats	NOAA	A	65°N	147°W	0 – 10000
ULB	Ulaanbaatar	NOAA	A	47°N	106°E	0 – 6000
HAA	Hawaii	NOAA	A	21°N	158°W	0 – 10000
RTA	Rarotonga	NOAA	A	21°S	160°E	0 – 10000

F = flask measurement
C = continuous (in-situ) measurement
C* = continuous (in-situ) measurement of CFC-12 and SF_6
A = aircraft flask measurement
[#] metres above sea level

Table 5. Calibration offsets relative to the NOAA2006A scale.

Site	Mean offset (ppb)
MHD	0.25
THD	-0.30
RPB	0.00
SMO	0.20
CGO	0.20

Table 6. Annual mean height of the tropopause (hPa) and the N_2O gradient (ppb) across the tropopause (cross-tropopause CT) and the 380 K isentrope. Tropics are defined as between 10°S and 10°N and extra-tropics are defined as latitudes higher than 30°.

	Tropopause height		CT gradient[a]		Gradient across 380K[b]	
	Tropics	Extra-tropics	Tropics	Extra-tropics	Tropics	Extra-tropics
MOZART4	103	239	1.0	0.6	1.0	4.2
ACTMt42l32	105	232	0.2	1.0	0.2	3.1
ACTMt42l67	106	233	0.1	0.9	0.1	3.3
TM5	105	233	2.6	1.3	2.6	5.5
TM3-NCEP	101	234	0.5	0.3	0.5	1.5
TM3-ERA	105	236	0.6	0.4	0.6	2.6
LMDZ4	109	226	6.2	0.3	6.2	8.0
TOMCAT	102	238	0.6	1.3	0.6	3.3

a. normalized to a CT pressure difference of 10 hPa
b. normalized to a pressure difference across the 380K isentrope of 10 hPa

Table 7. Annual mean (2006 – 2009) tropospheric growth rate, atmospheric lifetime, atmospheric abundance (up to 50 hPa) and global total sink of N_2O.

	Growth rate (ppb y^{-1})	Lifetime (y)	Abundance (TgN)	Sink (TgN y^{-1})
Observed	0.84	124 – 130*	-	-
MOZART4	0.99	128	1608	12.6
ACTMt42l32	0.52	92	1489	16.2
ACTMt42l67	0.84	119	1470	12.4
TM5	0.76	125	1544	12.4
TM3-NCEP	0.76	121	1515	12.5
TM3-ERA	0.86	126	1571	12.5
LMDZ4	0.24	119	1496	12.6
TOMCAT	0.86	108	1352	12.5

* Independent estimates of the lifetime (Prather et al., 2012; Volk et al., 1997)

Table 8. Correlations of modelled and observed zonal mean meridional gradients for different flux scenarios (mean 2006 – 2009). Also shown are the inter-hemispheric differences (IHD) calculated as the mean of values for all background sites north of 20°N minus the mean all of values for sites south of 20°S. The observed IHD for N_2O and SF_6 were 1.44 ppb and 0.36 ppt, respectively. R-values in brackets were not significant at the 95% confidence level.

Model	OCNPIC		OCNN04		OCNN95		BWMN04		SF_6	
	R	IHD	R	IHD	R	IHD	R	IHD	R	IHD
MOZART4	0.90	0.60	-	-	-	-	-	-	-	-
ACTMt42l32	0.89	1.00	0.88	1.01	0.85	1.09	0.85	0.96	-	-
ACTMt42l67	0.94	1.11	0.91	1.09	0.89	1.16	0.89	0.97	0.90	0.41
TM5	0.95	1.06	0.93	1.09	0.89	1.16	0.88	0.93	-	-
TM3-NCEP	(-0.04)	-0.18	(-0.26)	-0.27	(-0.27)	-0.20	(-0.42)	-0.31	-	-
TM3-ERA	0.91	0.72	0.85	0.72	0.81	0.79	0.79	0.56	0.99	0.39
LMDZ4	0.58	0.16	0.42	0.11	0.46	0.17	(0.02)	-0.01	0.91	0.69
TOMCAT	0.78	0.98	0.83	0.96	0.84	0.97	0.86	0.76	0.87	0.50

Table 9. Day of the year for the occurrence of the minimum in the mean seasonal cycle (2006 – 2009) of N_2O, CFC-12 and SF_6 at each of the background sites.

Model	Species	BRW	MHD	THD	MLO	SMO	CGO	SPO
Observed	N_2O	242	238	276	229	228	135	127
	CFC-12	232	232	217	201	217	113	139
	SF_6	266	254	248	215	246	39	50
MOZART4	N_2O	162	136	78	138	142	122	44
	CFC-12	-	-	-	-	-	-	-
	SF_6	-	-	-	-	-	-	-
ACTMt42l32	N_2O	189	181	169	141	235	123	185
	CFC-12	-	-	-	-	-	-	-
	SF_6	-	-	-	-	-	-	-
ACTMt42l67	N_2O	187	176	171	145	228	117	115
	CFC-12	223	233	211	143	270	90	95
	SF_6	242	241	219	43	186	40	55
TM5	N_2O	171	164	154	154	273	85	93
	CFC-12	-	-	-	-	-	-	-
	SF_6	-	-	-	-	-	-	-
TM3-NCEP	N_2O	136	123	122	125	243	253	173
	CFC-12	-	-	-	-	-	-	-
	SF_6	-	-	-	-	-	-	-
TM3-ERA	N_2O	169	152	156	150	250	59	75
	CFC-12	206	233	190	142	249	44	54
	SF_6	225	57	210	54	190	48	51
LMDZ4	N_2O	201	184	173	143	277	294	319
	CFC-12	183	316	170	182	41	149	60
	SF_6	211	239	189	231	276	41	38
TOMCAT	N_2O	167	131	133	178	323	127	97
	CFC-12	235	227	222	219	330	110	97
	SF_6	255	262	22	18	344	19	44

1 Fig. 1. Schematic of the TransCom-N_2O modelling protocol

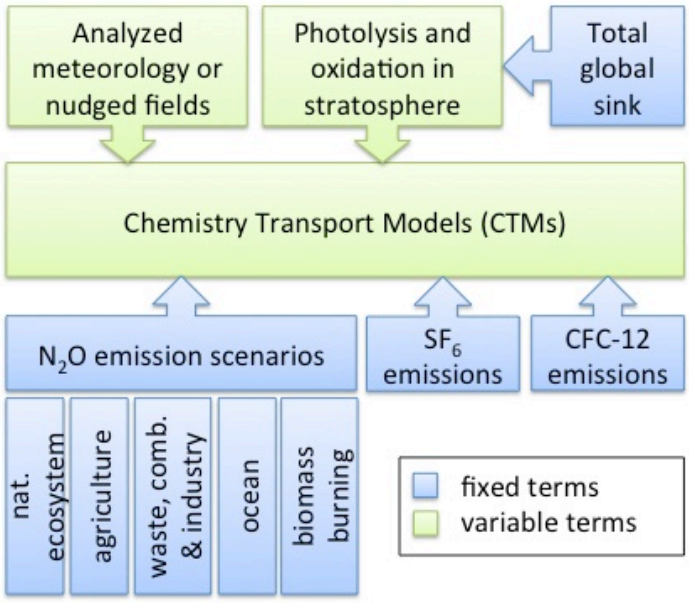

Fig. 2. Simulated zonal and annual mean latitude-altitude cross-sections of N_2O mixing ratio (ppb) from eight models shown for 2007. Superimposed are contours of annual mean potential temperature (K) (white lines) and mean tropopause height (black dotted line)

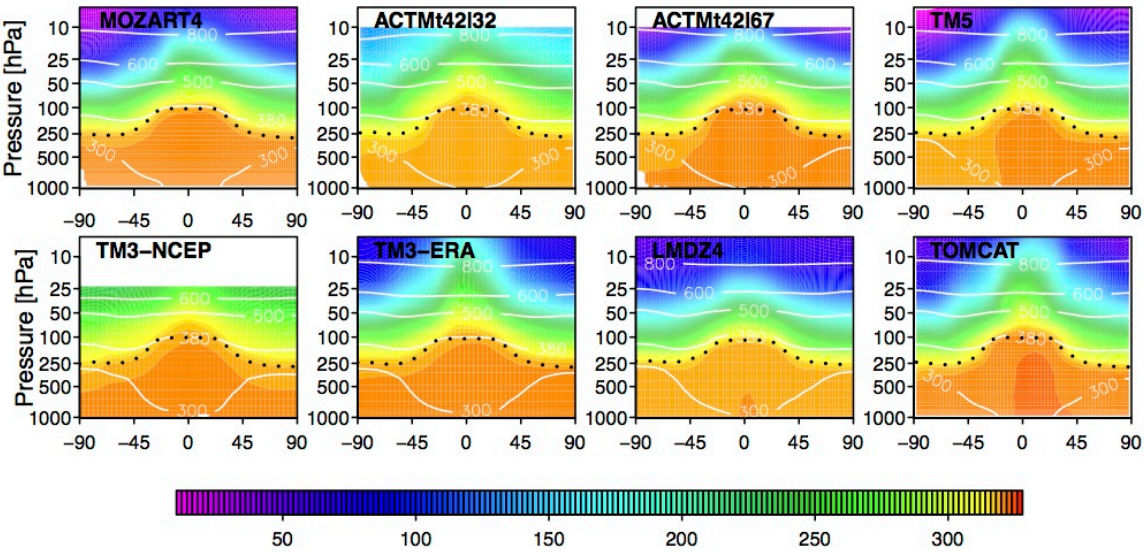

Fig. 3. Modelled and observed N_2O growth rates (ppb/y) versus lifetimes (y). Legend: Mozart4: yellow, ACTMt42l32: blue, ACTMt42l67: green, TM5: grey-blue, TM3-NCEP: purple, TM3-ERA: red, LMDZ4: magenta, TOMCAT: dark green, observed (covering the range of estimated lifetimes): black line.

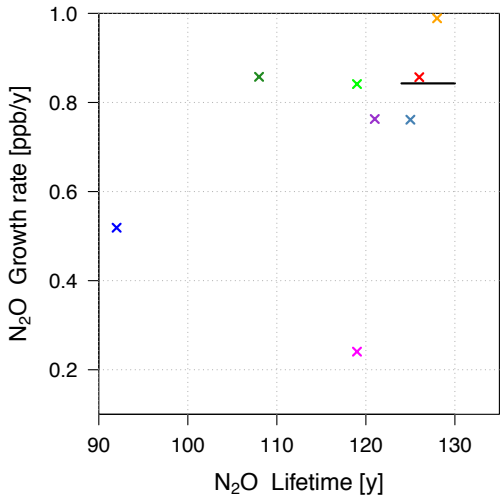

Fig 4. Vertical profiles of N_2O (ppb) at RTA, HAA, ULB and PFA (from top to bottom). The mean tropospheric mixing ratio at each site has been subtracted from the vertical profile. DJF = December, January, February; JJA = June, July, August; ANN = annual. Legend: Mozart4: yellow, ACTMt42l32: blue, ACTMt42l67: green, TM5: grey-blue, TM3-NCEP: purple, TM3-ERA: red, LMDZ4: magenta, TOMCAT: dark green, observed: black.

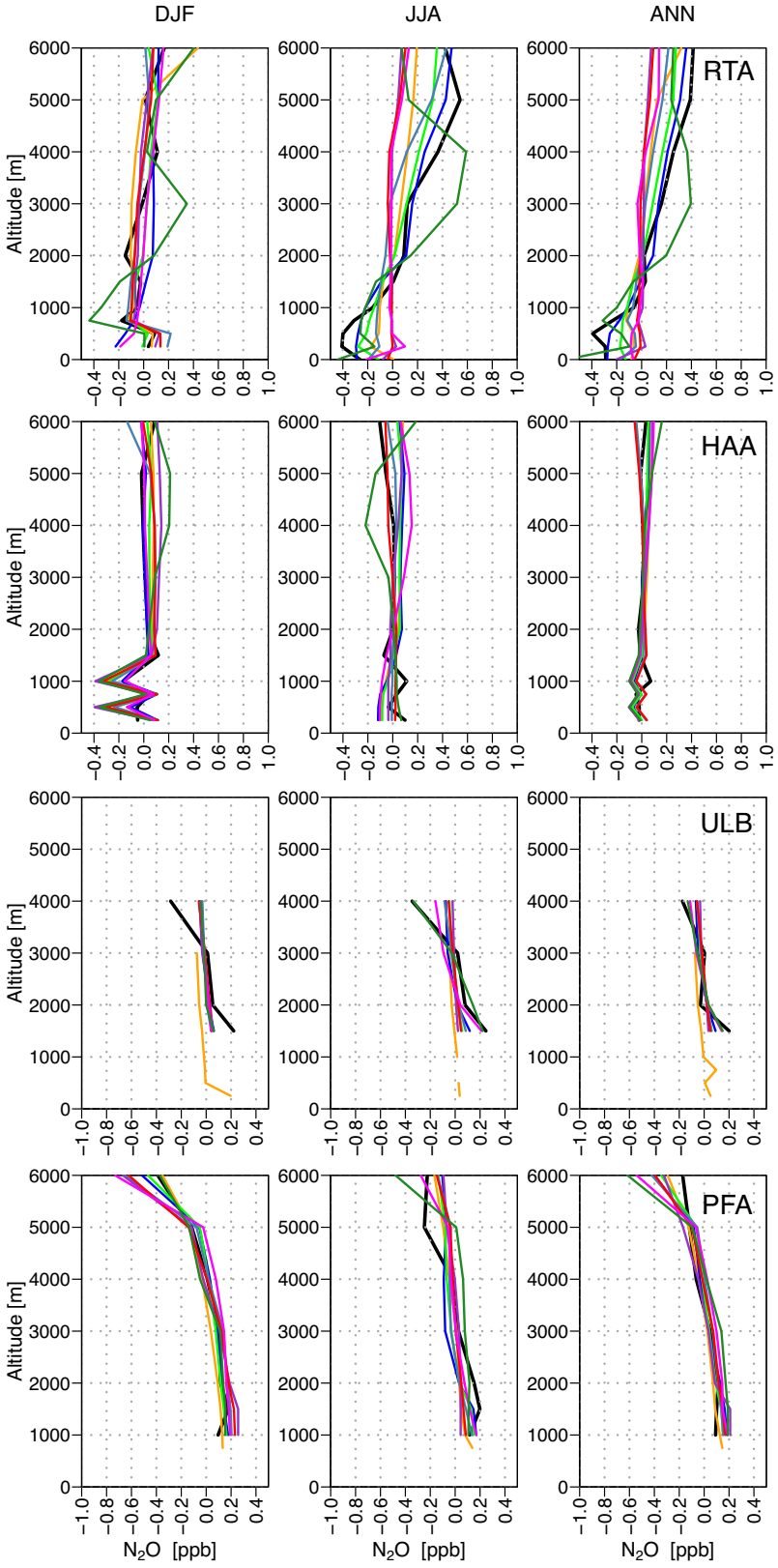

Fig. 5. Comparison of the meridional gradients of N_2O (left) and SF_6 (right) using the OCNPIC scenario. Shown are the annual mean mixing ratio at background surface sites (upper panel) and the total zonal and annual prior emission estimate (lower panel). Legend: Mozart4: yellow, ACTMt42l32: blue, ACTMt42l67: green, TM5: grey-blue, TM3-NCEP: purple, TM3-ERA: red, LMDZ4: magenta, TOMCAT: dark green, observed: black.

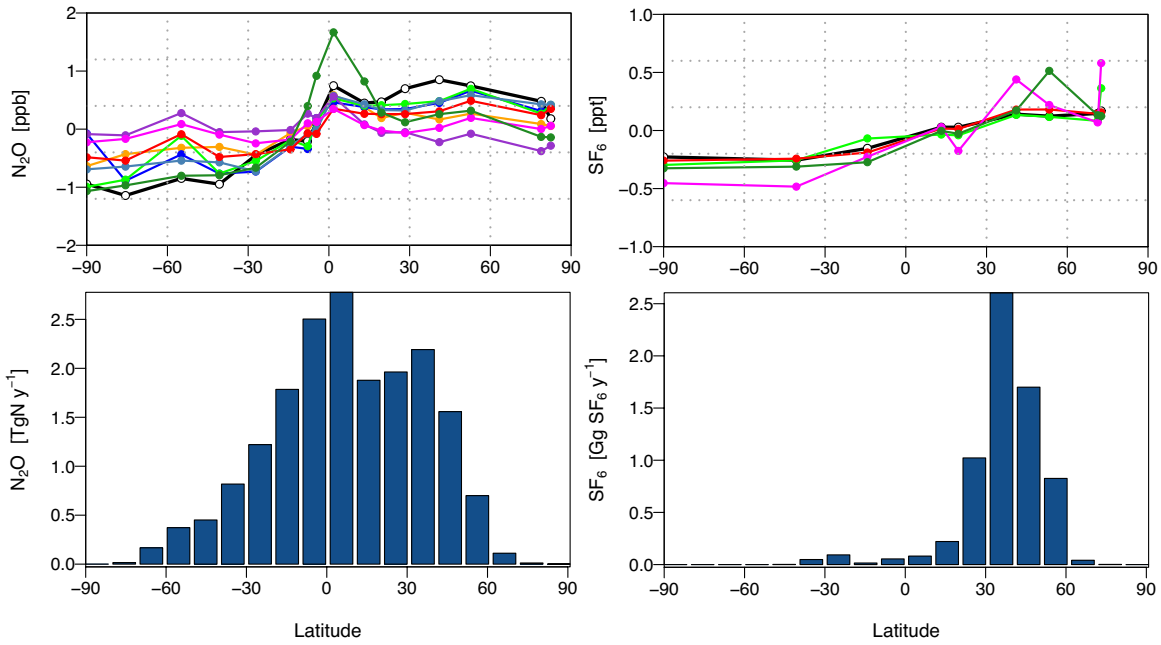

Fig. 6. Comparisons of modelled and observed north-south gradients of N_2O and SF_6. N_2O was simulated using the flux scenario, OCNPIC. Gradients are calculated as the mean of values for all background sites north of 20°N minus the mean of all values for sites south of 20°S. The left panel shows the N_2O (crosses) and SF_6 (circles) gradients for the observations and each model. The right panel shows the N_2O gradient versus the SF_6 gradient. Legend: Mozart4: yellow, ACTMt42l32: blue, ACTMt42l67: green, TM5: grey-blue, TM3-NCEP: purple, TM3-ERA: red, LMDZ4: magenta, TOMCAT: dark green, observed: black.

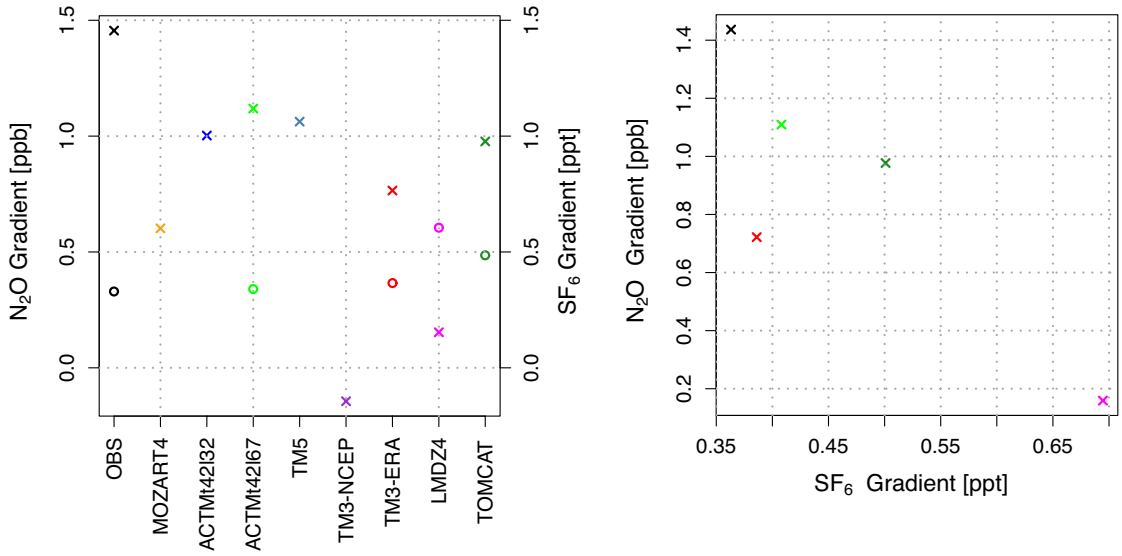

Fig. 7. Month of minimum in CFC-12 (upper panel) and N_2O (middle and lower panel) shown for each model (the subplots) in 2007.

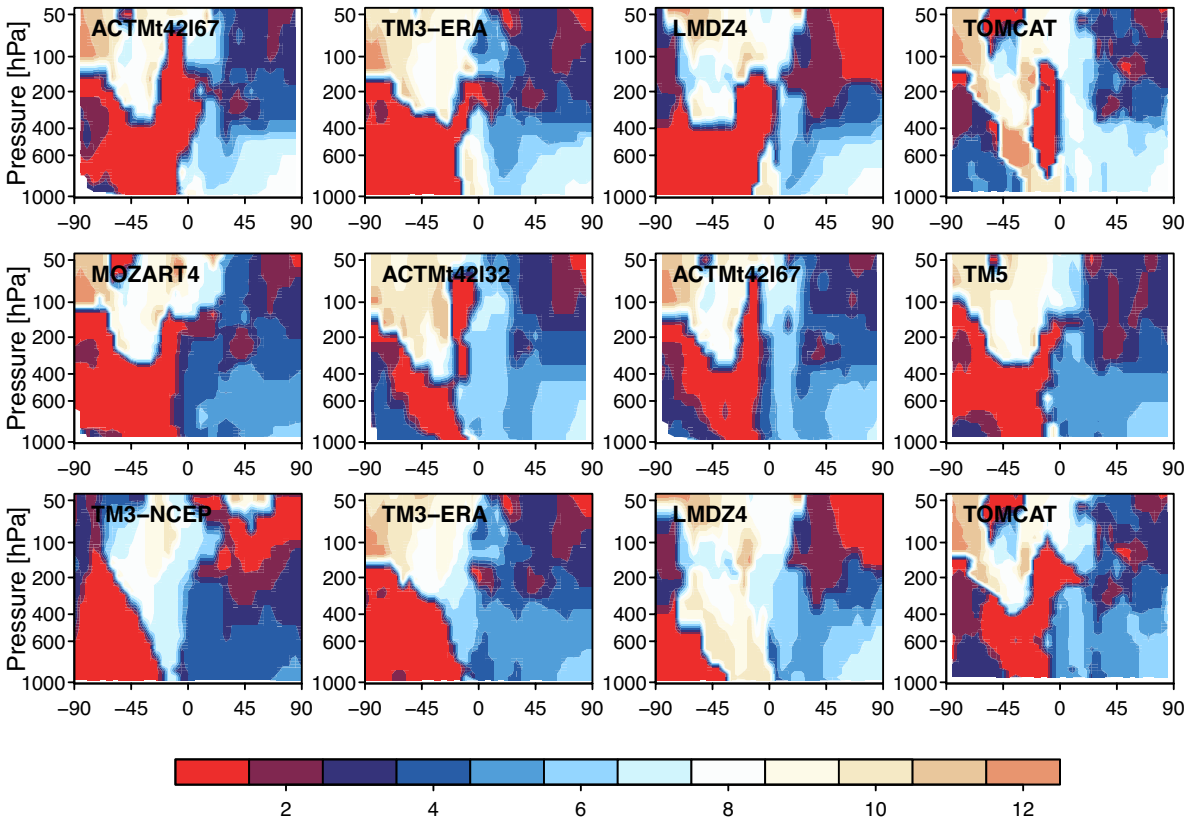

Fig. 8. Comparison of the climatological seasonal cycles (2006 – 2009) of N_2O (top row), CFC-12 (middle row) and SF_6 (bottom row) for selected background stations (each column). Legend: Mozart4: yellow, ACTMt42l32: blue, ACTMt42l67: green, TM5: grey-blue, TM3-NCEP: purple, TM3-ERA: red, LMDZ4: magenta, TOMCAT: dark green, observed: black.

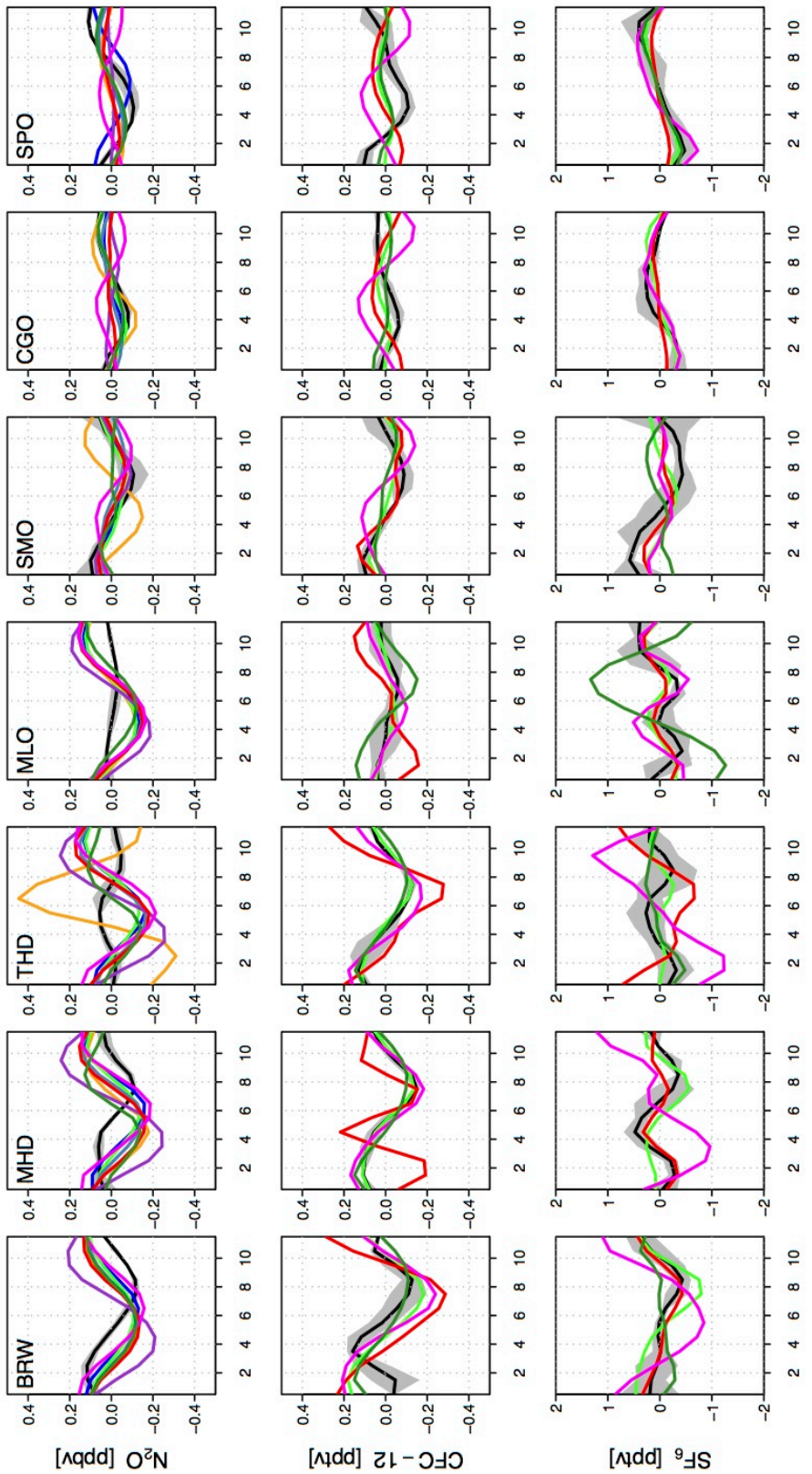

Fig. 9. Comparison of N_2O at different altitudes (along the rows) at the aircraft sampling sites: PFA (left panel), ULB (middle panel; no data were available for altitudes above 6000 m) and HAA (right panel). Data are shown as monthly means with the growth rates (as given in Table 6) subtracted. MOZART4 was adjusted with an offset of -1 ppb to fit the N_2O scale. Legend: Mozart4: yellow, ACTMt42l32: blue, ACTMt42l67: green, TM5: grey-blue, TM3-NCEP: purple, TM3-ERA: red, LMDZ4: magenta, TOMCAT: dark green, observed: black.

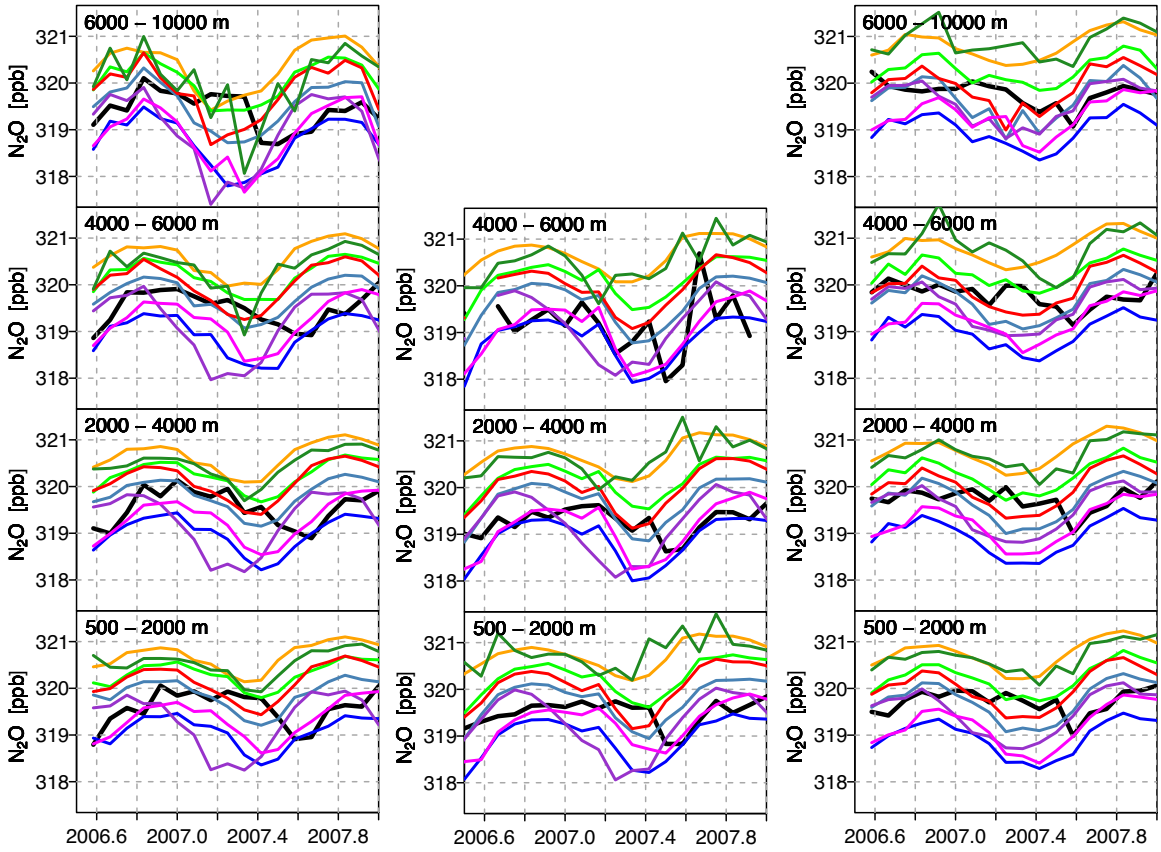

Fig. 10. Comparison of observed mean N_2O seasonality (2006 – 2009) with that modelled using 4 different prior flux models. Each station is shown as a separate panel and within each panel the 4 subplots are for each of the flux models as indicated in the top-left corner (see Tables 2 and 3 for a description of the fluxes). N_2O mixing ratio is on the left axis and N_2O flux (gray line) is on the right axis. Legend: Mozart4: yellow, ACTMt42l32: blue, ACTMt42l67: green, TM5: grey-blue, TM3-NCEP: purple, TM3-ERA: red, LMDZ4: magenta, TOMCAT: dark green, observed: black.

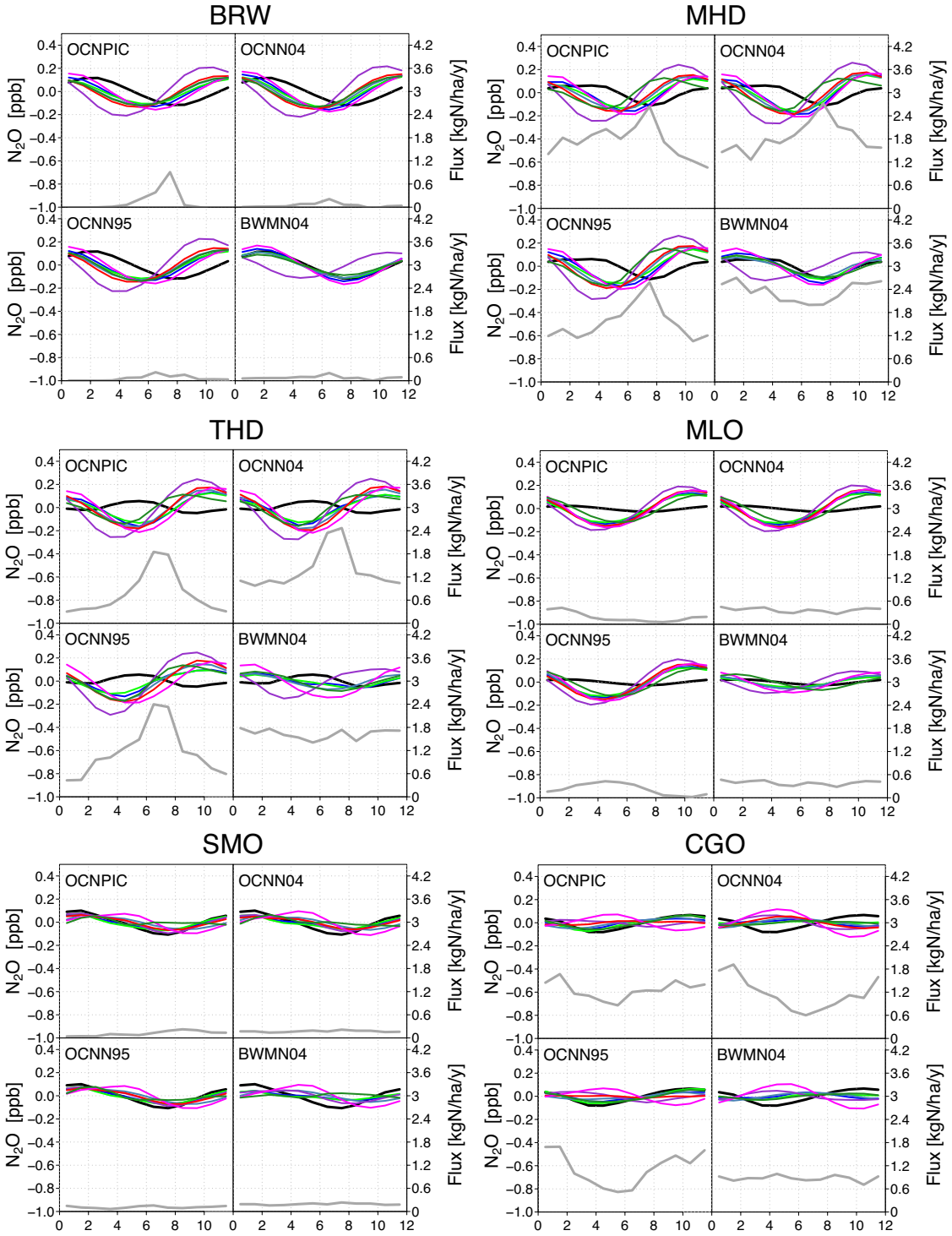

Supplementary Information

Fig. S1. Simulated zonal mean vertical profiles of N_2O mixing ratio (ppb) for DJF (upper panel) and JJA (lower panel) shown for each model as indicated in the top-left corner. Superimposed are contours of annual mean potential temperature (K) (white lines) and annual mean tropopause height (dotted black line).

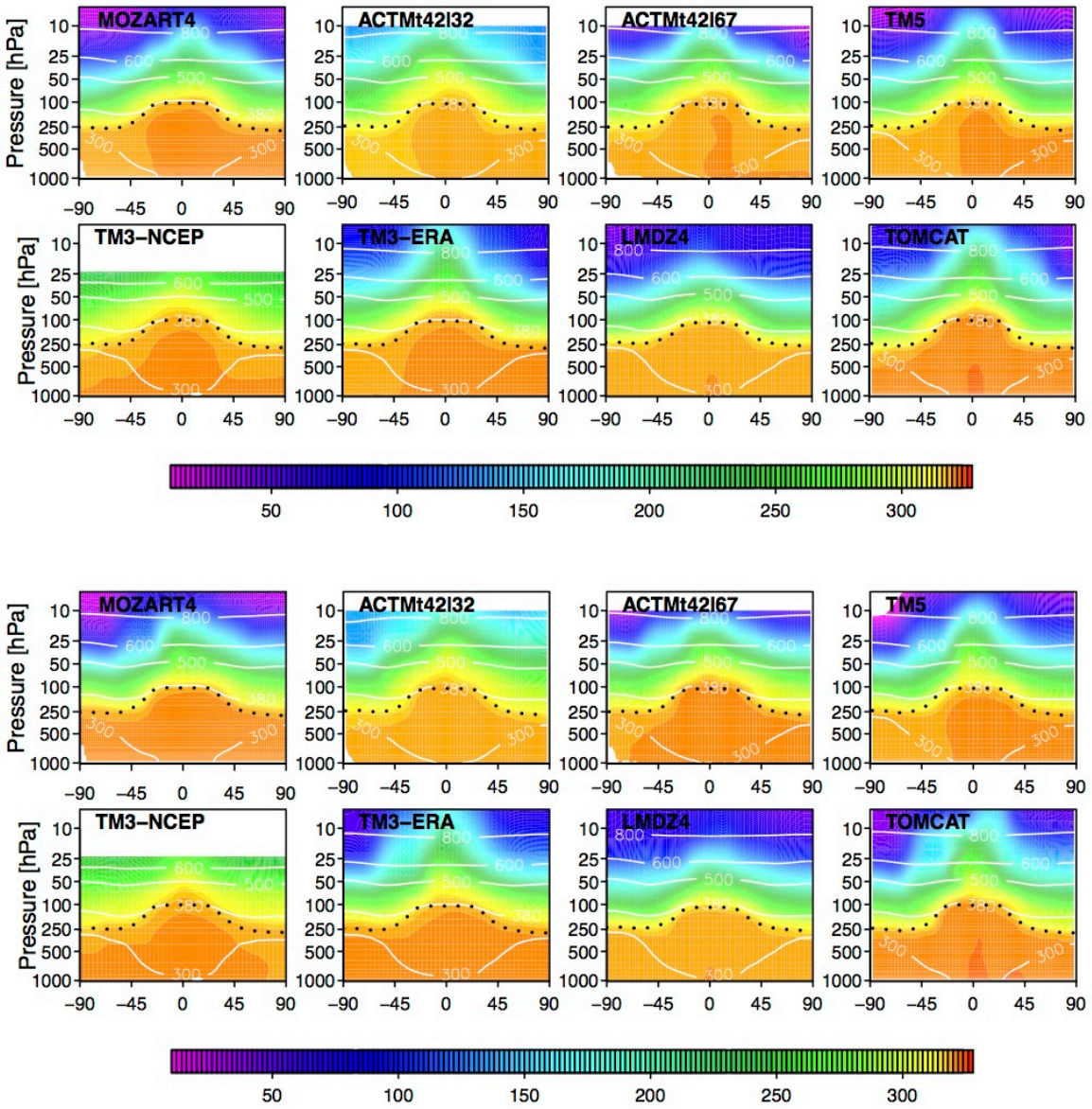

Fig. S2. Map showing the observations used in this inter-comparison study.

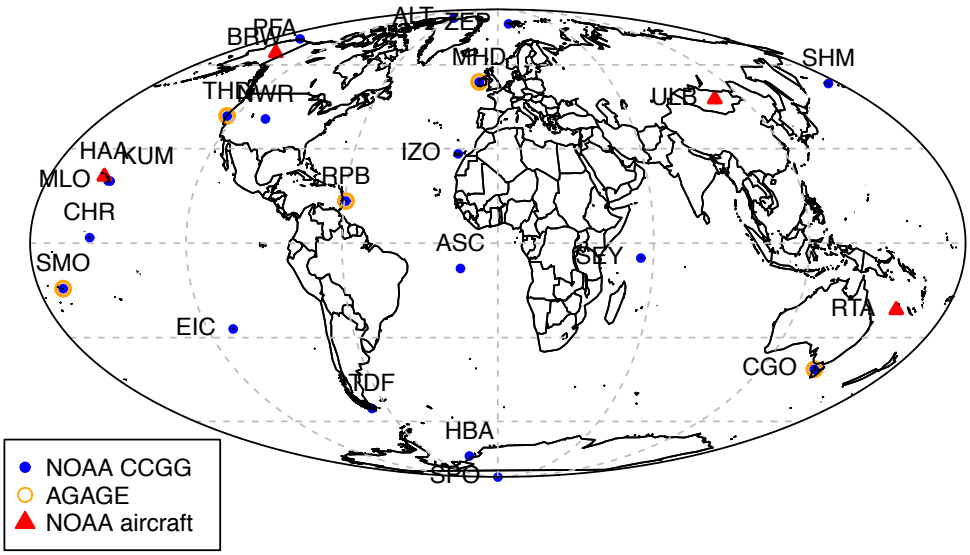

Fig. S3. Comparison of the zonal annual mean meridional gradients of N_2O (ppb) at the surface with the modelled/observed global mean mixing ratio subtracted. Shown are the gradients calculated using the flux scenarios: OCNPIC (top left), OCNN04 (top right), OCNN95 (bottom left), and BWMN04 (bottom right) with the integrated flux in 10° latitudinal bands (TgN y^{-1}) from each scenario shown in the bar-plot below. Legend: Mozart4: yellow, ACTMt42l32: blue, ACTMt42l67: green, TM5: grey-blue, TM3-NCEP: purple, TM3-ERA: red, LMDZ4: magenta, TOMCAT: dark green, observed: black.

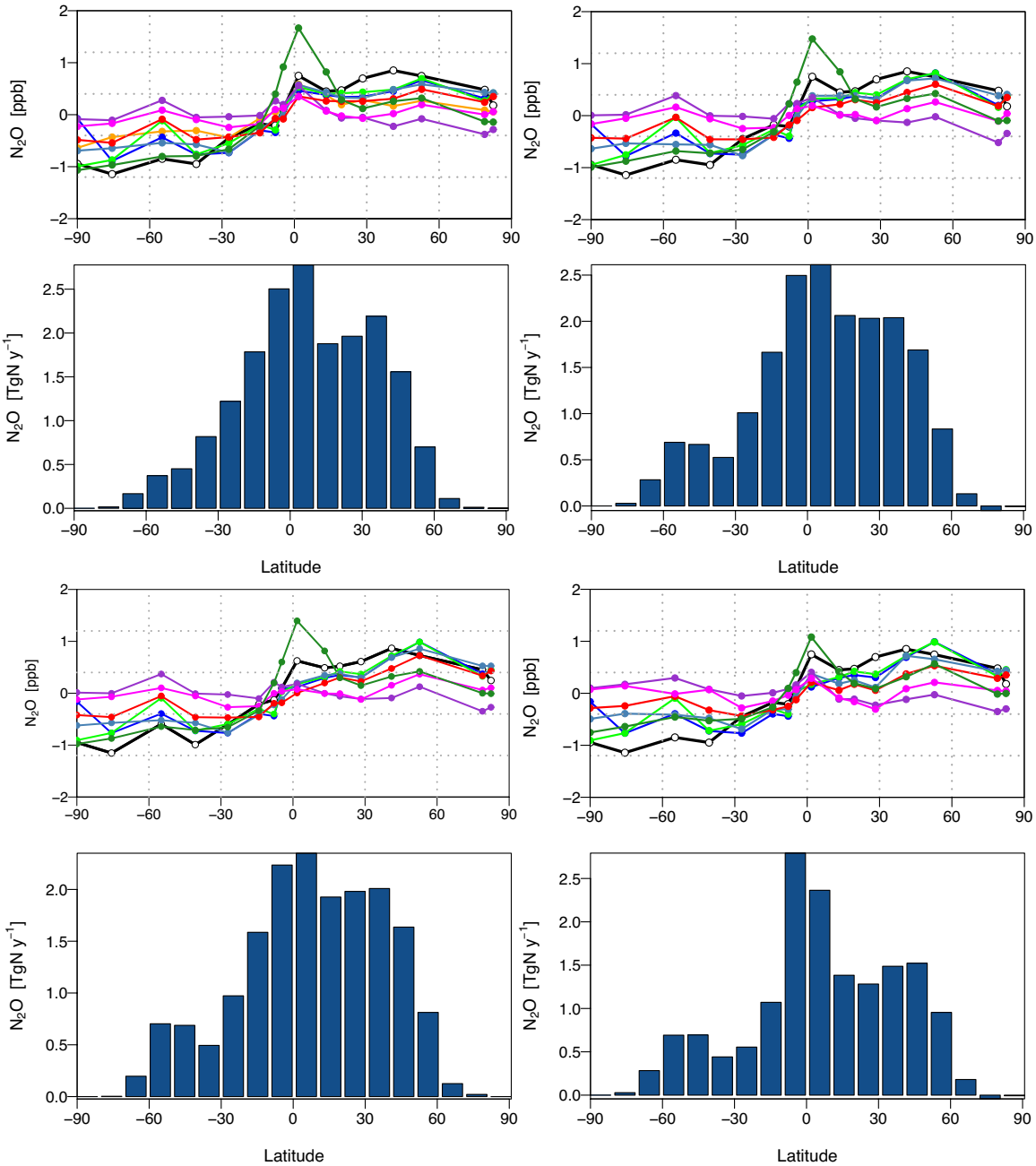

Fig. S4. Hovmöller plots of N_2O fluxes from the terrestrial biosphere in OCN (BWM had no seasonal cycle) and from the ocean in PIC, N95 and N04 (from top to bottom). Fluxes are shown in gN m^{-2} y^{-1}.